Planetary Science
a SpringerOpen Journal

ORIGINAL RESEARCH Open Access

Experimental and theoretical simulation of sublimating dusty water ice with implications for D/H ratios of water ice on Comets and Mars

John E Moores[1,2*], Robert H Brown[1], Dante S Lauretta[1] and Peter H Smith[1]

* Correspondence: john.e.moores@gmail.com
[1]Lunar and Planetary Laboratory, Department of Planetary Sciences, University of Arizona, 1629 E University Blvd, Tucson, AZ 85721-0092, USA
Full list of author information is available at the end of the article

Abstract

Sublimation experiments have been carried out to determine the effect of the mineral dust content of porous ices on the isotopic composition of the sublimate gas over medium (days to weeks) timescales. Whenever mineral dust of any kind was present, the D/H ratio of the sublimated gas was seen to decrease with time from the bulk ratio. Fractionations of up to 2.5 were observed for dust mixing ratios of 9 wt% and higher of JSC MARS-1 regolith simulant 1-10 μm crushed and sieved fraction. These favored the presence of the light isotope, H_2O, in the gas phase. The more dust was added to the mixture, the more pronounced was this effect. Theoretical modeling of gas migration within the porous samples and adsorption on the excavated dust grains was undertaken to explain the results. Adsorption onto the dust grains is able to explain the low D/H ratios in the sublimate gas if adsorption favors retention of HDO over H_2O. This leads to significant isotopic enrichment of HDO on the dust over time and depletion in the amount of HDO escaping the system as sublimate gas. This effect is significant for planetary bodies on which water moves mainly through the gas phase and a significant surface reservoir of dust may be found, such as on Comets and Mars. For each of these, inferences about the bulk water D/H ratio as inferred from gas phase measurements needs to be reassessed in light of the volatile cycling history of each body.

PACS codes: 98.80.Ft [Isotopes, abundances and evolution (astronomy)], 64.70.Hz [Sublimation], 68.43.-h [Adsorption at solid surfaces]

Keywords: Stable Isotope Geochemistry, Sublimation, Icy Bodies, Adsorption of Water, Comets, Mars

Background

Motivations for simulating HDO

The deuterium to hydrogen ratio (D/H) of water is often used to infer the evolution of water inventories on planetary bodies [for instance, [1,2]]. It is a particularly effective tool for several reasons. First, the signatures of D and H-bearing molecules can be detected and distinguished spectroscopically [3,4] in the atmospheres of other planets. Secondly, there is a high potential for large mass-dependant fractionations upon dissociation as D and H have the largest mass difference of any isotope pair, with D being twice as massive as H. This must be considered along with the tendency of terrestrial planetary atmospheres to evolve towards more oxidated states as hydrogen is lost to

space through Jeans escape from the atmospheric exobase [2]. If the water inventory of the planet is exchangeable with the atmosphere, the signature of this missing hydrogen will be partly preserved in the remaining water reservoir as a large enrichment in D/H.

This argument is often used to assert that planetary bodies with elevated D/H ratios in their present day-atmospheres lost most of their water during the early evolution of their atmospheres [5]. However, there are two important caveats to this conclusion. First, in order to assess the amount of fractionation it is necessary to make estimates of the initial D/H values of the reservoir in question [1]. This is a difficult task even for the bulk solar system as the initial store of deuterium in the solar system's largest reservoir, the Sun, was consumed early in the life of the solar system. The protosolar value can be obtained through analysis of the Jovian atmosphere and solar wind implanted isotopes [6], however, this remains more difficult for specific bodies. For instance, while [7] argues for a primitive origin for comets, two distinct reservoirs with different D/H ratios are required to explain the observed values.

The second caveat is that fractionation of the major planetary water reservoirs is not ongoing in the present era, i.e. since the surface and climate evolved to its present state. As a result, explanations for large variations in the observed D/H ratios between different Solar System bodies, such as the 5.5-fold enrichment of the heavy isotope seen in the Martian atmosphere [3,4] compared to VSMOW (Vienna Standard Mean Ocean Water) or the 15-fold enrichments in comets [8-10] compared to protosolar values [6,10] have largely ignored whether the enhanced signal observed is the result of a bulk loss of water, or simply a byproduct of cycling at cold temperatures in the presence of large quantities of dust. Given the fractionations that are possible on the Earth during volatile cycling between reservoirs [11], it is important to quantify this effect.

The isotopic fractionation of water ice during sublimation on planetary bodies has been considered a simple temperature-driven process in which colder ices tended to fractionate more heavily than warmer ones due to the differences in lattice binding energy between H_2O and HDO [12-16]. This energy difference results in lower equilibrium sublimation pressures for HDO, the more refractory form of water, and intensifies at lower temperatures, increasing the relative refractory nature of HDO compared to H_2O. Typically, when this information is applied to planet-scale analyses, either just this equilibrium value has been used [17] or is first combined with the concept of a static lattice in which no fractionation occurs due to a buildup of the more refractory isotope on the surface until the ice sublimates at the bulk ratio [18].

Recent work on the simulation of sublimation and fractionation of water ice

Additionally, recent laboratory experiments have shown that the sublimation of water ice is not a simple and steady process, and that D/H ratios in the vapor can be time variable, mimicking to a degree the Rayleigh-like fractionation seen in the evaporation of liquids [19]. Previous experimental work [20] provides a good summary also indicates that realistic samples containing mixtures of ices or contaminating dusts can severely impact the sublimation rate and isotopic character of the escaping gas. The observations of the KOSI (Kometen Simulation) experiments [21-28], designed to simulate sublimation on cometary bodies, are particularly relevant to the work to be described in this paper.

The KOSI experiments were a major initiative to understand the processes that affect comets and are made up of eleven individual experiments conducted at the DLR Institute of Space Simulation, Cologne. Collectively, these experiments examined many different compositions of comets and ice/dust ratios [20]. However, there are two areas where these experiments need to be extended in order to examine the long-term isotopic behavior of samples. First, none of the KOSI experiments lasted longer than 59 hours. Secondly, only two of the experiments, KOSI-7 and KOSI-11, used isotopic tracers and only KOSI-11 employed any HDO enrichment [20]. As such, even though there is data on the isotopic character of some of the remaining sample condensate [29] there are no D/H profiles of the sublimate gas available to identify how the sample changes with time.

This paper will fill this gap by considering the isotopic medium-term evolution of dusty ice. The results of an experimental investigation into the sublimation of realistic samples of porous, disaggregated and dusty ices will be described in order to study the evolution of fractionation between the solid and gas with time. Additionally, some theory about how realistic samples of ice will fractionate in planetary settings will be discussed as well as the implications that the results have for the evolution of Comets and the polar caps of Mars. Definitions of all variables used in this analysis are presented in Table 1.

Methods

Experimental Apparatus

The experimental apparatus is detailed in [19]. This setup, shown schematically in Figure 1, consists of a vacuum-jacketed cryostat in which samples can be cooled from below by a closed-cycle helium cooler attached to a 1/2-inch copper thermal capacitor and heated from above by a Quartz-Tungsten-Halogen (QTH) lamp which produces a blackbody spectrum and was run at powers between 1 and 4 W. The chamber has a volume of 150 cm^3 with a cross-sectional area of 10 cm^2 and typically contained 50 cm^3 of sample. 3 silicon diode temperature sensors were located on the outside of the thin-walled chamber wall within the vacuum jacket. A high vacuum was maintained within the inner sample chamber with the turbomolecular pump of a Quadrupole Mass Spectrometer (QMS-100) atmospheric sampler from Stanford Research Systems. This instrument had a capacity of 20 liters per second at operational pressures, as verified by a calibrated helium leak. For initial evacuation a second Pfeiffer turbomolecular pump was operated on a separate line. This allowed the main analysis line to remain as pristine as possible. Several pressure measurement devices were located on this line including a 20mtorr capacitance manometer near the chamber. At the QMS-100 inlet, a cold cathode gauge verified the pressure measured just inside the QMS-100 using a Stanford Research Systems RGA-100 residual gas analyzer quadrupole mass spectrometer. By monitoring the partial pressures of masses 17-22 (primarily $H^{16}O$ through $D_2{}^{18}O$) the D/H ratio of the gas escaping the sample chamber could be measured.

Experimental procedure

A typical run consisted of three stages: sample preparation, sample insertion and sample observation. Sample preparation involved mixing measured volumes of H_2O and

Table 1 Summary of symbols used in equations

Symbol	Units	Definition
A	molec s kg^{-1}	Constant from Equation (1.a)
A_{surf}	m^2	Surface area of the frozen sample
A_S	m^2 kg-1	Specific surface area of the regolith available for adsorption
α	Pa^{-1}	Langmuir adsorption constant (subscripts refer to the species)
B	m^3 $molec^{-1}$	Constant from Equation (1.b)
C	kg m $molec^{-1}$ s^{-1}	Constant from Equation (1.c)
χ	dimensionless	Mass fraction (subscripts: Z = of dust; H2O = of water)
D_{eff}	m^2s^{-1}	Diffusivity (subscripts: eff = Effective Diffusivity; 0 = time independent) When bolded represents a 2- element vector with [H_2O HDO]
e_{sys}	dimensionless	Pumping efficiency (pressure ratio between chamber and QMS-inlet)
G	dimensionless	Rate coefficient matrix
γ_Z	dimensionless	Volume fraction of dust in lag mantle
k	dimensionless	Rate constant, Superscripts: ads = adsorption, des = desorption, X = cross-reaction substitution by vapor-phase species. When bolded represents a 2- element vector with [H_2O HDO]
k_B	m^2 kg s^{-2} K^{-1}	Boltzmann Constant (1.38×10^{-23})
J	molec m^{-2} s^{-1}	Molecular flux at a point in the apparatus
k	s^{-1}	Langmuir adsorption kinetic constant, Subscripts: H2O, HDO, X = substitution; Superscripts: ads = adsorption, des = desorption
l	m	Thickness of an adsorbed monolayer of water (2.75×10^{-10})
m_{H2O}	kg $molec^{-1}$	Mass of a single water molecule (2.99×10^{-26})
M_{H2O}	kg mol^{-1}	Molar Mass (0.01802 for water)
N_A	molec mol^{-1}	Avogadro's Number (6.02×10^{23})
n	molec m^{-3}	Number density of molecules
p	Pa	Pressure (subscripts: sat = Saturated Vapor Pressure)
R	$m^2K^{-1}s^{-2}$	Specific Gas Constant (462 for water)
R_u	J mol^{-1} K^{-1}	Universal Gas Constant (8.3145)
ρ	kg m^{-3}	Density (subscripts: Z = of dust; reg = of regolith; H2O = of water)
Ψ	J m^{-3}	Thermodynamic Adsorption Constant
T	K	Temperature (subscripts: QMS = the tubing at the throat of the QMS)
t	s	Time (subscripts: 0 = initial time)
θ	dimensionless	Fraction of adsorption sites occupied by water molecules when bolded indicates a two-element vector with [H_2O HDO]
V	m^3 s^{-1}	Pumping speed
z	m	Thickness of dust lag (subscripts: 0 = initial time)

D_2O together with a measured mass of dry mineral dust samples (hereafter described as "dust"). Typically, 50 mL samples were prepared by combining 47.5 mL of H_2O with 2.5 mL of D_2O yielding an initial D/H ratio of 0.053 with the deuterated species present almost entirely as HDO due to rapid proton transfer. This liquid was then combined directly with an appropriate mass of dry dust to achieve the desired mass fraction, shaking well to incorporate all the components thoroughly. The properties of the dust used will be described in the "Dust and regolith simulants" section.

Sample insertion procedures evolved over the course of the experimental runs; however, differences in preparation do not appear to have had a noticeable effect on the results based on blank samples (see Section "Dust and regolith simulants"). Early on, the sample chamber was filled with liquid nitrogen (LN2) and the liquid water-dust

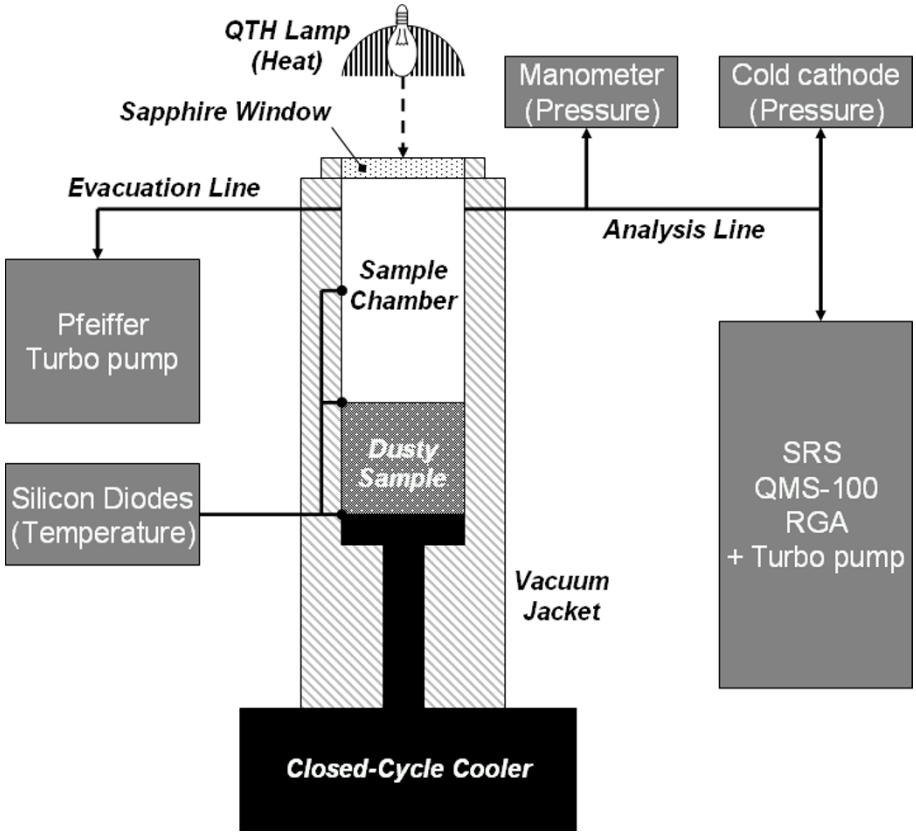

Figure 1 Schematic of Experimental apparatus showing major gas plumbing and sensors. The volume of the sample chamber is approximately 150 cm^3.

mixture created during sample preparation was poured directly into the chamber in small amounts, shaking the remaining liquid between pours. Later on, a step was added in which small amounts of the prepared liquid were poured into a mortar filled with LN2 where the resulting dusty ice was crushed to sand-sized particles using a pestle. This water-dust-LN2 slurry was then transferred to the waiting LN2-filled sample chamber. The advantage of the additional step was that it produced a more even surface layer as the sand sized particles settled in the LN2.

LN2 was used as a medium for two reasons. First it was able to rapidly freeze and cool the ice-dust liquid mixtures before growing ice crystals were able to exclude the dust particles. Microscopy of prepared ices (Figure 2) shows that the dust is well incorporated into the final icy samples created using this method. Several different ice crystal morphologies were observed (e.g. hexagonal, banded, rounded grains) depending on the dust concentration, however the rounded textures shown in Figure 2 were the most common. Secondly, LN2 boil-off during sample freezing prevented room air from condensing on the samples, hence preventing contamination by isotopically light water.

Once the samples were inserted in the sample chamber, but before the LN2 had evaporated, a relief valve on the sample chamber was closed and the sapphire observation window placed upon its gasket. This allowed the sapphire to act as a pressure relief on the sample chamber without admitting room air until the nitrogen had evaporated. Once the nitrogen pressure had decreased to almost atmospheric pressure, the window

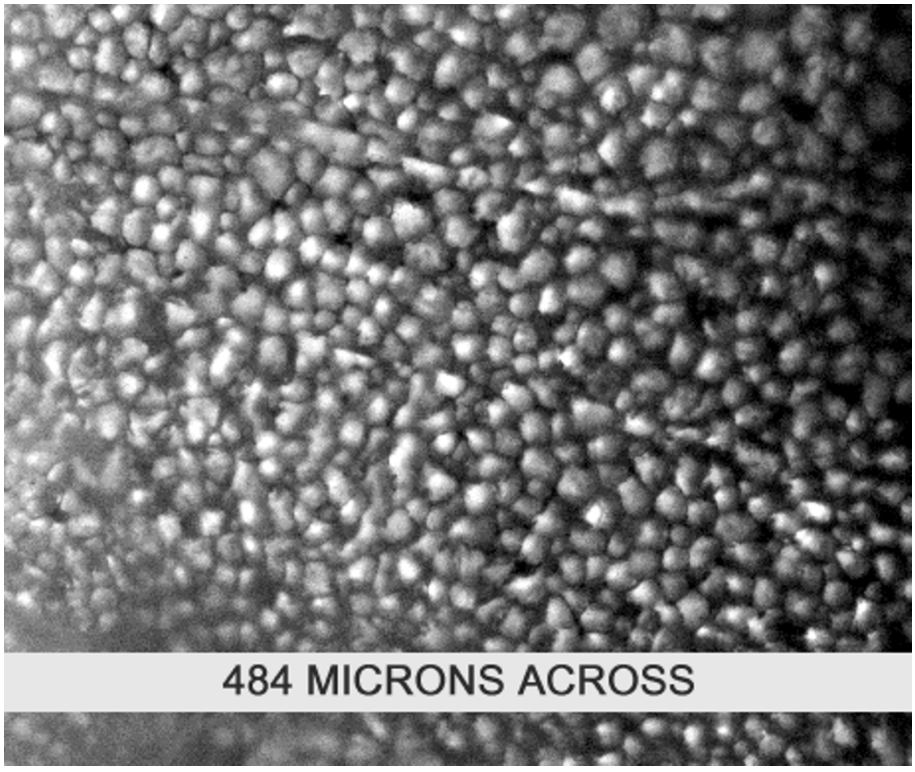

Figure 2 Microscopy of 25 wt% 1.5 μm diameter TiO_2 dust in water ice following flash freezing in LN2. The ice grains formed are ~20 μm across and are separated by a matrix of the finer dust. Generally, lower concentrations of dust produced larger characteristic grain sizes.

was clamped down onto its gasket and a blow-down line was opened. This procedure cleaned the sample and removed any residual nitrogen. To remove any solid nitrogen created by this evacuation, the temperature of the base of the sample (hereafter referred to as "basal" temperature) was temporarily increased to 150 K. Note that the basal temperature is simply an experimental parameter. It is not the bulk temperature of the sample and not representative of the temperature of the actively sublimating surface. The actual temperature of the surface is most directly determined by the initial gas pressure and related to the basal temperature only by the thermal conductivity of the sample.

While the sample was being cleaned by the blow-down line, a background mass spectra was obtained on the valved-off analysis line by averaging 30 minutes worth of observations. This procedure was repeated after the experiment was concluded. Both observations were combined to provide an average background to be removed from the observed values of pressure for each species during the experimental run. Typical background values for the water group, masses 18 to 22, were between 1×10^{-9} torr and 2×10^{-8} torr with the light isotope $H_2{}^{16}O$, mass-18, being the largest component.

Finally, once a sufficiently low pressure had been achieved in the chamber (typically a few days), the sample observation phase could begin. At this point, the blow-down line would be shut, the analysis line opened up, and the lamp moved into position and turned on. Logging of all sensor outputs including all three temperature sensors, the basal temperature, the 20mTorr and cold cathode pressure gauges as well as the partial

pressures of all species from the QMS would also be started. Generally, no external changes were permitted over the course of an experimental run.

During this stage, [19] operated with temperatures at the base of the sample near 150 K when dealing with solid ice samples to produce surface temperatures of 200-210 K. However, since more porous samples were employed here, lower basal temperatures were required, of order 60-120 K in order to produce the same surface temperatures and to maintain the QMS in its preferred linear range at or below 5×10^{-5} torr at the QMS inlet.

Dust and regolith simulants

Not including the blanks which contained no dust, five separate compositions and sizes of dusts and regolith simulants were used. These were: (a) Titanium (IV) Oxide (TiO_2 Rutile) in 1-2 μm sized particles (b) Silicon Dioxide in 1-2 μm sized particles (c) cuttings from the Fukang Pallasite in 1-50 μm sized particles (d) dry sieved JSC Mars-1 Regolith Simulant 76-105 μm sized particles and (e) crushed and water settled JSC Mars-1 Regolith Simulant 1-10 μm sized particles. Simulants (a) through (c) were used to achieve a broad understanding of the apparatus, to outline the effect of dust on samples and to perform blank runs without dust. These samples were chosen mainly for their availability and not as analogues for realistic planetary dust analogues. However, this paper will focus mainly on results from the last two simulants since these represent realistic planetary analogues for the Martian polar caps. It should be noted, however, that all dust stimulants exhibited similar trends (see Section "Comparison to other dust compositions and blank runs").

JSC Mars-1 is a standard martian regolith simulant noted as spectrally and chemically similar to observations on the martian surface and consists of water-modified glassy volcanic ash collected from the Pu'u Nene cinder cone on the island of Hawaii [30]. The material is primarily SiO_2 (43.7 wt%) Al_2O_3 (23.4 wt%) and Fe_2O_3 (11.8 wt%) with smaller amounts of CaO (6.2 wt%), TiO_2 (3.8 wt%), FeO (3.5 wt%) and MgO (3.4 wt%) in addition to trace constituents.

Production of dust (d) from this material was straightforward using a sieving machine. However, in order to obtain dust (e), a grain size representative of martian airfall dust, it was first necessary to process the sieved JSC Mars-1. The grain size of martian airfall dust comes from the 1.6 μm radius particle peak of the distribution of dust observed in the martian atmosphere from landed spacecraft, as determined by studies of the martian atmosphere [31-33]. This material was produced by taking raw JSC Mars-1 and crushing it using a mortar and pestle before pouring the resulting detritus into a 10 cm deep water settling tank for 30 minutes. Those particles still in suspension were poured off along with the water and were desiccated and collected as chips. Microscopy confirmed the expected grain size distribution of particles up to 10 μm in diameter. However, the composition of this material was not assayed following collection and may be slightly different from the proportions for bulk JSC Mars-1 shown above.

Note that smaller-grained materials, such as the carbon particles employed in the KOSI experiments [20], were not attempted due to concerns that they could be lofted into the tubing from the sample chamber and into the QMS inlet, potentially damaging the mass spectrometer.

Sources of error

There are several potential sources of error for any particular D/H value to be reported. The largest uncertainty is in the partial pressures of the various species measured by the Quadrupole Mass Spectrometer (QMS). Measurements are taken of the entire mass spectrum every minute which means that a large number of points are associated with any run. Since the rate of the change of the pressure is typically slow, it is possible to perform a statistical analysis on the individual measurements over a few hours to derive 1-σ errors for the D/H ratio, these are shown in Table 2 and range from 0.7% to 6.9% of the total value.

There could also be uncertainty in the preparation of samples; however, this is expected to be smaller. All liquid samples were prepared using calibrated volumetric pipettes. Furthermore, rapidly frozen mixtures of HDO and H_2O have not been found to fractionate significantly, especially when the freezing is rapid [34,35]. Nevertheless, the final values of the D/H ratio were compared to the initial value obtained at the start of the experiment during which the surfaces of the samples were unprocessed and should have been sublimating at close to their bulk isotopic ratios.

Results

The experimental runs conducted are summarized in Table 2 which lists the grain size of dust, the dust mixing ratio, duration, basal temperature, the greatest 1-σ error in the D/H ratio, typically at the end of the run, and the maximum fractionation factor. The fractionation factor is the ratio between the bulk D/H ratio of the original solid and the observed minimum gas D/H ratio.

Typical pressure and temperature profiles

A typical pressure and temperature profile from the dusty samples is seen in Figure 3, plotting the outputs of the 20 mtorr manometer and the Temperature sensor located at a height of 5 cm above the base of the sample chamber. This temperature sensor is located close to the sample surface, but likely is in poor thermal contact with the sample due to the high porosity of the sample. This likely explains the low temperature reported which should be between 181 K and 207 K, assuming saturation in the chamber and the pressure range seen in the upper panel.

An important feature is the decline in pressure which continues for the duration of the experiment. This decline is accompanied by a stable temperature regime which suggests changes occurring in the sample itself. This type of a pressure decline has been seen previously in crystalline experiments [19] and is a well documented feature

Table 2 List of palagonite experimental runs

Run	*Grain Size*	*Dust Content*	*Duration*	*Basal T*	*1-σ D/H Error*	*max fractionation*
7	1-10 μm	1 wt%	7.8 days	60 K	5.2×10^{-4}	1.0
8A	1-10 μm	3 wt%	12.8 days	60 K	6.6×10^{-4}	1.2
8B*	1-10 μm	3 wt%	7.0 days	60 K	6.5×10^{-4}	1.1
9	1-10 μm	6 wt%	17.8 days	60 K	1.4×10^{-3}	1.2
10	1-10 μm	9 wt%	19.6 days	60 K	1.9×10^{-3}	1.9
11	1-10 μm	25 wt%	36.0 days	60 K	1.3×10^{-3}	2.7(1.6)
12	105-150 μm	9 wt%	15.6 days	60 K	3.7×10^{-3}	1.0

*Following Excavation of topmost layer

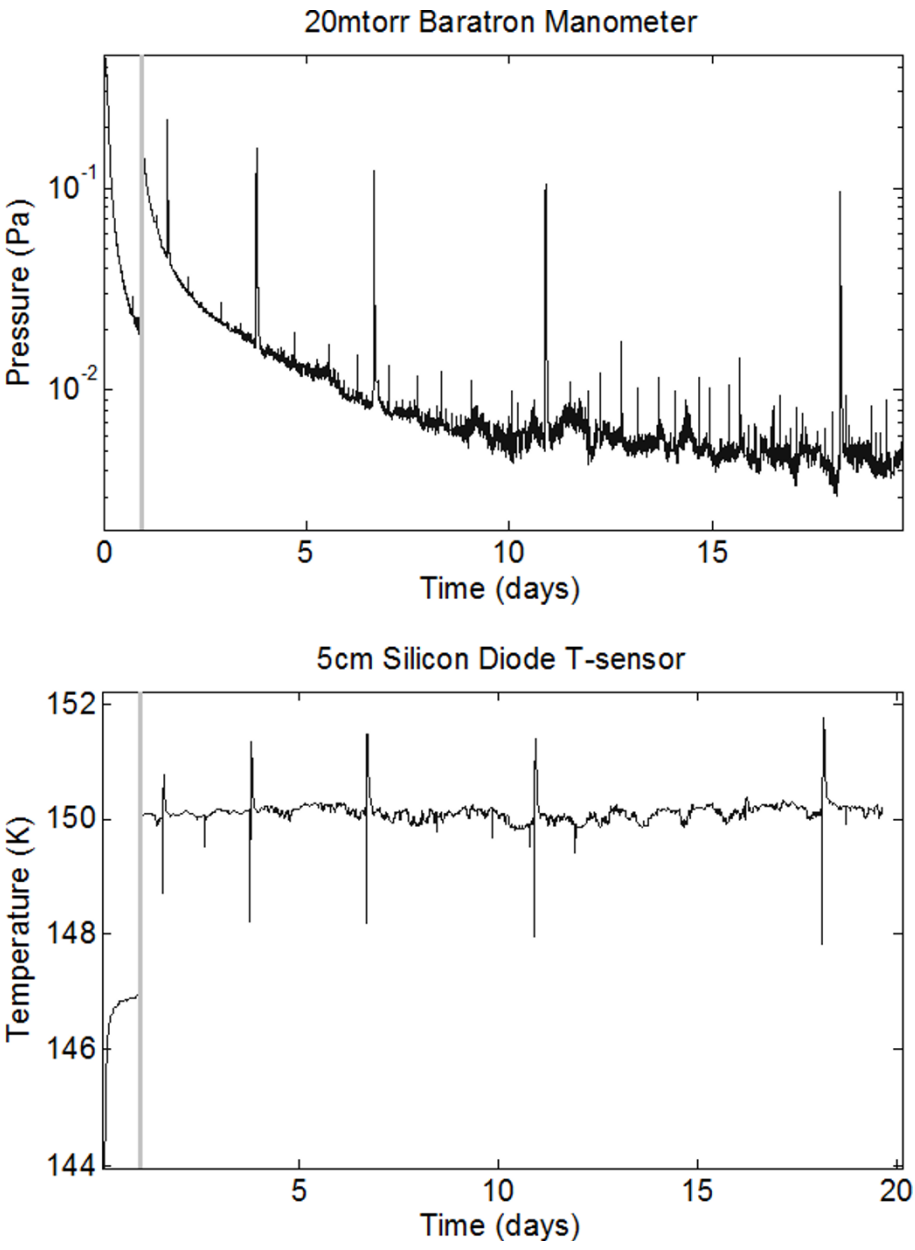

Figure 3 Evolution of the pressure at the 20mtorr manometer and the temperature sensor near the sample surface for the run described in Figure 4, panel E. The time of first illumination by the lamp is given by a vertical grey bar. Note the large decrease in pressure observed over the course of the run compared to a lack of an appreciable temperature change.

of the dusty KOSI experiments [20]. In the KOSI experiments, the pressure decline observed was assumed to be the result of the formation of a dusty lag layer [36]. This possibility will be discussed further in Section "Discussion".

For several reasons, it seems unlikely that the decrease in pressure is caused by the gradual removal of adsorbed water on the interior surfaces of the chamber and lines. First, the analysis line was maintained at a high vacuum at all times and was heated between runs to drive off any adsorbed water. Background measurements detected contamination from water at the level of only 2×10^{-8} torr, more than three orders of

magnitude lower than the lowest pressure observed during any experimental run. Furthermore, since the sample chamber contains a water ice sample which is directly heated from above, it seems unlikely that the walls which contain only adsorbed water and were not heated, would contribute a greater signal by several orders of magnitude. But most tellingly, the D/H profile for such a process is opposite to what would be expected. The end of each sample run produced the most HDO-poor gas and it would be this gas which would be expected to remain on the surface of any plumbing. Next, during sample replacement, very HDO-poor room air was permitted to enter the sample chamber while the chamber was at room temperature. If either of these sources was contributing heavily to the D/H ratio of gas emitted from the chamber, one would expect the initial D/H ratio to be low and to increase as this interfering contamination became exhausted. Instead, the opposite trend is observed (see Sections "Palagonite series" and "Comparison to other dust compositions and blank runs").

Next, a discontinuity is observed at 1 day of elapsed time. This corresponds to turning on the Quartz-Tungsten-Halogen (QTH) lamp to provide heat directly to the surface of the sample. As expected, this event corresponds to sudden increases in the temperature and pressure. Immediately following this event, both signals return to their initial tendencies: a decline in pressure at the manometer, and a stable temperature signal. Since the temperature stabilizes within ten minutes, thermal equilibrium is achieved quickly.

The last significant feature is the presence of five large spikes in pressure and temperature at declining intervals. These large excursions are similar in structure to the events termed "sublimation cascades" in [19] and seen in several different experimental apparatuses. As in [19] we observe that these events are accompanied by excursions in the D/H ratio of the sublimating samples, however, their contribution to the overall proportions of HDO and H_2O sublimated is small and therefore can be neglected when considering the trends in the D/H ratio.

Palagonite series

Overview

Figure 4 shows seven experimental runs in which the dust content varies from 1 wt% in panel A through 3 wt% in panel B and C, 6 wt% in panel D, 9 wt% in panel E and 25 wt% in panel F. Panel C demonstrates the effect of removing 1 cm of overburden from the surface of a sample which had been sublimating for 13 days. This removal was accomplished by opening the sample chamber, backfilling with LN2 and removing the upper part of the sample with a spatula and was completed within a few minutes. Panel G examines the effect of changing the size of dust particles, from 1-10 μm to 76-105 μm, while holding the mass concentration constant at 9 wt%. As dust concentration is described as a mass mixing ratio, this final experiment provided a way to separate the effect of particle size, and hence the specific surface area since larger particles have less surface area per unit mass, of the particulates on the sublimating ice.

This last panel also illustrates the response of samples to changing illumination conditions. At day 1 and again just prior to day 15, the intensity of the lamp was increased as a step. The immediate response of the D/H ratio was to increase as well. This is also observed for all the other palagonites, particularly the lower wt%, but not for the 25 wt

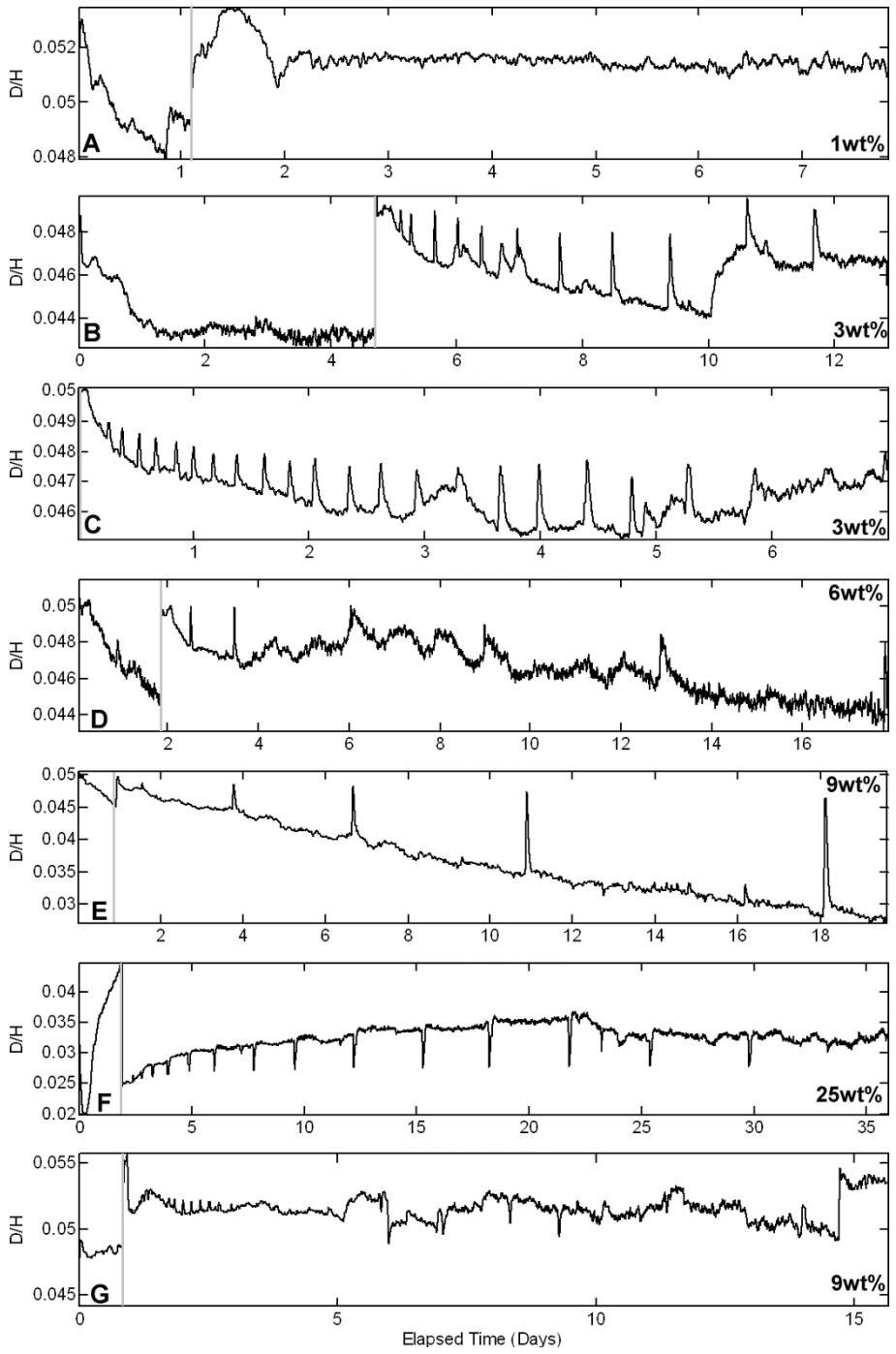

Figure 4 Palagonite series, note differences in the x and y scale between panels. The time of first illumination by the lamp is given by a vertical grey bar. From top to bottom 1 wt% 1-10 μm particles, 3 wt% 1-10 μm particles, 3 wt% 1-10 μm particles following excavation of the top 1 cm of sample, 6 wt% 1-10 μm particles, 9 wt% 1-10 μm particles, 25 wt% 1-10 μm particles, 9 wt% 76-105 μm particles Only dust contents 9 wt% and 25 wt% are heavily fractionated by the end of their runs, while all ices contaminated with fine dusts show some degree of increasing fractionation with time.

% sample which saw a decrease in the D/H ratio of the sublimate gas upon being illuminated.

In many cases, as mentioned in section "Typical pressure and temperature profiles", the initial pressure in the chamber exceeded the maximum pressure at the RGA. As such, it was necessary to wait until the pressure had declined sufficiently before beginning the illumination. This process took from a few hours to 5 days depending upon the particular sample in question. As a result there is an initial large jump in pressure which often shows up as a large jump in the D/H ratio within the first five days of each run that corresponds to this event, such as just before day 5 in panel B, day 2 in panel D, day 1 in panel E, day 2 in panel F and day 1 in panel G. A clear jump due to this effect cannot be discerned in panel A, and panel C represents a continuation of panel B–therefore it is fair to say that the jump occurs between the two runs. Note that the lamp is first turned on at 27 hours (1.13 days).

A trend in dust

From this series of experiments it is possible to discern a trend in the amount and speed with which fractionation of the sublimated gas takes place. The lowest dust concentration, 1 wt%, is shown in Figure 4, panel A, and shows almost no fractionation. Instead, the D/H ratio remains stable at 0.052, near the bulk ratio after an initial excursion following first illumination just after 1 day. At 3 wt% (panels B and C) it is possible to discern a slight downward trend in the D/H ratio bottoming out around 0.045 by the end of the run. Interestingly, there seem to be several fractionation reverses despite the appearance of somewhat stable pressure behavior. Most notably these occur at day 10 in panel B and around day 3 in panel C. As mentioned above, panel C describes the sample following the removal of the top centimeter of material. From the initial high D/H value at the start of the run shown in panel C it appears that, at depth, the sample remains unfractionated. However, once this surface is exposed it begins to fractionate just as the original surface had in panel B. At 6 wt% (panel D) the fractionation becomes slightly more pronounced, with D/H declining to 0.044 by the end of the run. At 9 wt%, the D/H value declines to 0.028 by the end of the run, a fractionation factor of 1.9. This run exhibits the largest end-time fractionation of any run completed.

After 9 wt% the dust content was increased to 25 wt%. This sample (shown in panel F) exhibited a different behavior compared to samples with lower dust contents. The sample began to fractionate heavily prior to the day 2 lamp illumination. This fractionation was reversed after peaking at a factor of 2.5, with the D/H ratio ascending up to 0.045. The lamp illumination, instead of being accompanied by a spike in the D/H ratio is instead shown as a sudden decrease of D/H down to 0.025. By the end of the run, D/H had increased only to 0.032, an apparent asymptote, sublimating during the entire run at D/H values much lower than the bulk. This suggests that this heavy fractionation may be a long term effect and not simply transitory. The specific elements of the 25 wt% case which differ from the 9 wt% case and a possible explanation for both are discussed more fully in the Section "Using adsorption to explain a special case".

The final panel of Figure 4 describes the effect of replacing the 1-10 μm particles of the 9 wt% case with 76-105 μm particles. The degree of fractionation is much less than the 1-10 μm case. The result is a run that shares many aspects of behavior with

the 1 wt% case. This is suggestive that the fractionation may be related to the total surface area of dust available and not to the mass of dust.

Comparison to other dust compositions and blank runs

Since experiments with JSC MARS-1 palagonite dusts were more extensive than those with other dusts, these have been used to illustrate the trend of increasing D/H fractionation with increasing dust content. However, it is noteworthy that similar D/H profiles were obtained from all dusts mentioned in the Section "Dust and regolith simulants". Furthermore, blank runs which contained no dust and which were prepared in an analogous manner to the runs which contained dust, showed no significant fractionation during runs of over 30 days. Both sets of observations are presented in Figure 5 with significant fractionation observed on SiO_2 with D/H values observed down to 0.03 (Panel C), and on TiO_2 with D/H values down to 0.02 (Panel D). Less fractionation was observed on the Pallasite cuttings (Panel E). This effect is possibly due to the larger size of these cuttings when compared to the palagonites, SiO_2 and TiO_2.

Discussion

Pressure decline

A possible cause: dust lag formation

The decline in pressure observed in all samples over time is puzzling when considered in light of temperature readings which are essentially constant. Typically, for a sublimating sample, these two variables are highly correlated–in equilibrium sublimation, it is the temperature which uniquely determines the pressure in the sample head space. As such, starting pressures, ending pressures and the corresponding temperature of the sublimating surface, assuming a saturated equilibrium in the chamber, are given in Table 3. Graphically, a typical pressure decline is shown in Figure 3 along with the corresponding temperature trace for the 9 wt% palagonite.

It is noteworthy that this kind of profile can also be seen in previous work. The KOSI-9 experiment in which the dust to ice ratio was 0.11 (9.9 wt%) is a particularly good example. Here, over a three hour stretch where the illumination was held constant, the flux of escaping particles increases, peaks and begins to fall before the lamp power is reduced [27]. Unfortunately, the lamp output does not remain constant for long enough to determine the nature of this pressure profile.

Thus, it seems likely that the increased surface area of the disaggregated samples and possible reorganization of pathways through the sample may explain the larger scale of the declines. The most straightforward way for a dusty sample to produce these pathways is through the formation of a dust lag. Such a lag creates a diffusive barrier to sublimation which can lead to a decline in the observed sublimation rate. This is what had been assumed to have occurred in the KOSI simulations [27] and was modeled by [36]. As such, the pressure decline that would be expected is documented in the following section and our results are compared to those of [36].

Quantifying putative dust lag formation

Before determining how great a barrier this dust mantle is to escaping particles, it is necessary to calculate the amount of dust lag that is expected from a sublimating sample. Typical rates of sublimation seen in dusty runs are of order 10 μm day^{-1} of clean

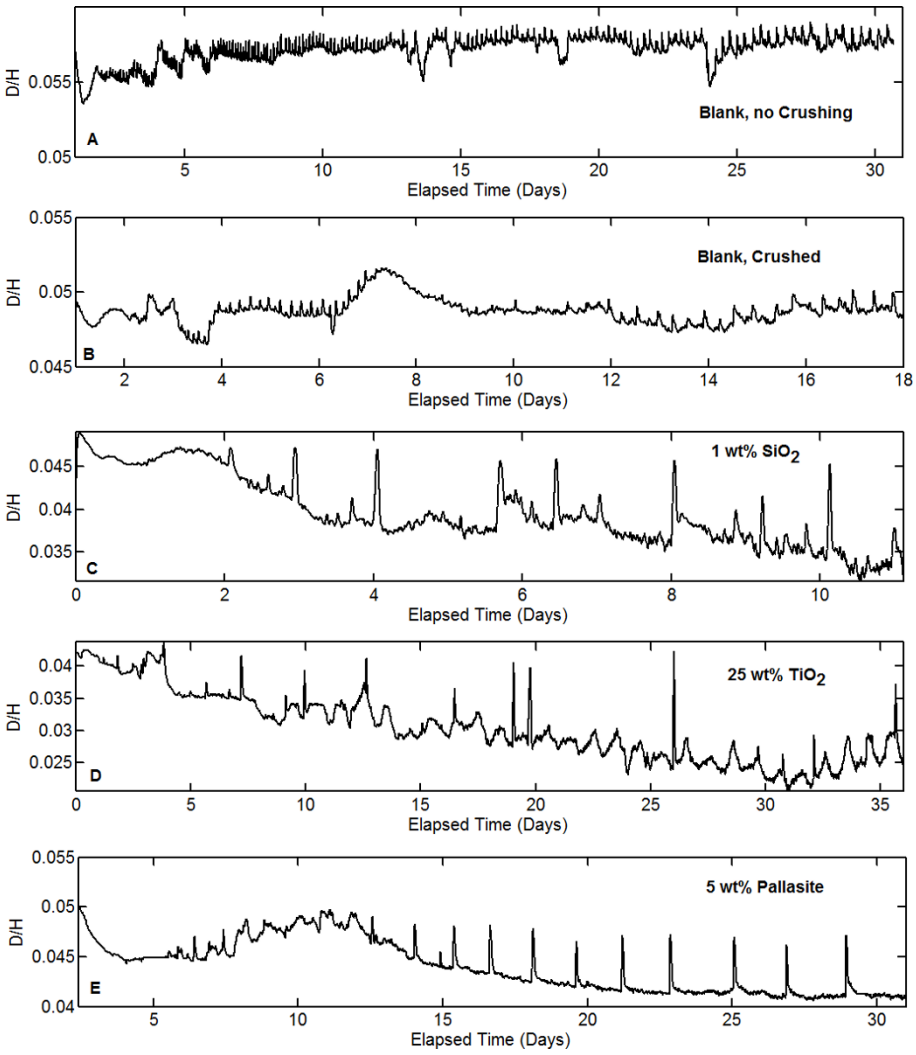

Figure 5 Blank Runs and other dusts. Lamp illumination occurred near the start time shown for all runs. (**A**) A blank (no dust) prepared by pipetting water into LN2 in the sample chamber or (**B**) pipetting water into LN2 outside the chamber and crushing with a mortar and pestle. Neither blank shows a significant fractionation; however, they give an idea of the degree of non-uniformity of disaggregated samples. Mixtures prepared analogously to panel B, but with different dusts are shown in the bottom three panels. These dusts are (**C**) 1 wt% SiO_2 in 1-2 μm particles (**D**) 25 wt% TiO_2 in 1-2 μm particles and (**E**) 5 wt% cuttings from the Fukang Pallasite in 1-50 μm particles. All three dusts show some increase in fractionation over time.

Table 3 Pressure/temperature decay parameters for palagonite runs

Run	P_{START} *(mtorr)*	T_{SURF}* *(K)*	P_{END} *(mtorr)*	T_{SURF}* *(K)*
0**	11	216	0.53	195
7	2.5	205	0.21	189
8A	2.7	206	0.060	182
8B	3.0	207	0.18	189
9	3.5	207	0.049	181
10	2.9	206	0.040	180
11	4.8	210	0.034	179
12	6.6	212	0.043	181

*Based on Starting/Ending Pressure (Saturation Assumed) may not be representative of the actual temperature
**Slowly frozen ice from [20]

ice equivalent. If it is assumed that the excavated dust is loosely packed with porosities approaching 50%, typical for bulk JSC Mars-1 [30] then the thickness of lag creation should vary from 0.08 μm day^{-1} to 2.7 μm day^{-1} for 1 wt% to 25 wt% dust mixing ratios, respectively. The rate of lag creation will vary over time, thus it is useful to look at the total lag built up by the end of the run. This is estimated based on the total mass of material sublimated and tabulated in columns 2 and 3 of Table 4.

The speed of diffusion of water molecules will also be affected by the temperature of this dust lag. For this variable, it will be assumed that the lag does not vary in temperature over its thickness and is the same temperature as the sublimating surface. This is reasonable given the estimates of lag thicknesses which are less than 228 μm in all cases at all times. This thickness when combined with reasonable assumptions regarding the thermal conductivity suggest that the temperature drop across the lags will be less than 0.01 K.

Using this information, the thickness of the lag at any time (and the corresponding chamber pressure) can be calculated by solving the following equations. First, Fick's first law for the molecular flux (molecules m^{-2} s^{-1}) in terms of pressure can be expressed as:

$$J|_{diffusion} = -D_{eff}\frac{\partial}{\partial z}\left(\frac{p}{m_{H2O}RT}\right) \cong \frac{-D_{eff}}{m_{H2O}TR}\frac{\Delta p}{\Delta z} = A\frac{(p_{sat}-p)}{\Delta z} \quad (1.a)$$

Where the temperature has been separated from the derivative as the temperature drop across the lag layer is expected to be small and m_{H2O} refers to the mass of a single water molecule. D_{eff} is the observed diffusivity in m^2s^{-1}, z is the lag thickness in m, p is the pressure in Pa, T the temperature in K and R is the specific gas constant for water of 462 m^2K^{-1} s^{-2}. All constant terms are absorbed into A for simplicity, and p_{sat} is the vapor pressure of the ice at the actively sublimating surface below the lag. Note that all variables used in this analysis and all the analysis to follow in this paper are defined in Table 1. As water molecules are evaporated, the lag will thicken according to:

$$\frac{dz}{dt} = J\frac{M_{H2O}}{N_A}\frac{\chi_Z}{\chi_{H2O}}\frac{1}{\rho_Z\gamma_Z} = BJ \quad (1.b)$$

Where M_m is the molar mass of water, N_A is Avogadro's number, χ_Z and χ_{H2O} are the mass fractions of dust and water, respectively, ρ_Z is the density of dust, and γ_Z is the proportion of the volume of lag that is dust, as opposed to open space. As before,

Table 4 Dust lag and diffusion timescales for 1-10 μm palagonite series

Run	*H_2O_{Eq} Layer*	*Estimated Lag Thickness*	*C_{KOSI} (m kg^{-1} $s^{-0.5}$)*	*Mantle Diffusivity*	*R^2*	*Effective Pore Radius**
7	536.8 μm	6.78 μm	1.3×10^{19}	$2.0 \times 10^{-7}m^2s^{-1}$	0.95	2.8×10^{-10}m
8A	421.3 μm	16.3 μm	2.8×10^{18}	$2.9 \times 10^{-8}m^2s^{-1}$	0.76	4.0×10^{-11}m
8B	325.4 μm	12.5 μm	1.6×10^{18}	$8.9 \times 10^{-9}m^2s^{-1}$	0.79	1.2×10^{-11}m
9	408.8 μm	32.6 μm	1.9×10^{18}	$2.5 \times 10^{-8}m^2s^{-1}$	0.77	3.5×10^{-11}m
10	250.2 μm	30.9 μm	1.2×10^{18}	$1.5 \times 10^{-8}m^2s^{-1}$	0.67	2.1×10^{-11}m
11	547.0 μm	228 μm	2.7×10^{18}	$2.1 \times 10^{-7}m^2s^{-1}$	0.42	2.9×10^{-10}m
12	1017 μm	126 μm	5.5×10^{18}	$3.3 \times 10^{-7}m^2s^{-1}$	0.75	4.5×10^{-10}m

*Assuming that the pressure decline can only be explained without considering adsorption

constant terms are absorbed into the constant B. Finally, using the parameters of the setup, we may relate the flux of escaping particles to the pressure in the chamber by:

$$p = J\frac{k_B T_{QMS} A_{surf}}{e_{sys}\dot{V}} = CJ \tag{1.c}$$

Where k_B is Boltzmann's constant, T_{QMS} is the temperature of the tubing at the throat of the QMS, taken to be equal to the room temperature of 295 K, A_{surf} is the surface area of the sample, e_{sys} is the efficiency of the system (the ratio between the pressure at the throat of the QMS and in the chamber, nearly a constant 0.01 over the pressures involved) and the final constant is the pumping speed of the system, a nearly constant 0.02 $m^3\ s^{-1}$ (20 L s^{-1}). Note that in the limit of a system with completely free sublimation the back pressure tends towards zero.

Solving these three equations yields expressions for the escaping flux of particles, chamber pressure and the lag thickness in terms of t, the time elapsed:

$$z(t) = \sqrt{A^2C^2 + z_0^2 + 2ACz_0 + 2p_{sat}AB(t - t_0)} - AC \tag{2.a}$$

$$p(t) = \frac{ACp_{sat}}{\sqrt{A^2C^2 + z_0^2 + 2ACz_0 + 2p_{sat}AB(t - t_0)}} \tag{2.b}$$

$$J(t) = \frac{Ap_{sat}}{\sqrt{A^2C^2 + z_0^2 + 2ACz_0 + 2p_{sat}AB(t - t_0)}} \tag{2.c}$$

where z_0 is the thickness of the lag at $t = t_0$ and accounts for any lag which has accrued from insertion of the sample and chamber pump-down. As t becomes large compared to the initial conditions, the chamber-specific constant, C, disappears and the flux of particles approaches:

$$J(t) = \frac{Ap_{sat}}{\sqrt{2p_{sat}AB(t - t_0)}} \tag{3.a}$$

This form is similar to the decrease in pressure due to dust mantling observed during the KOSI experiments and modeled by [36] whose expression for the escape rate can be given as:

$$J_{KOSI}(t) = \frac{C_{KOSI}\rho}{2\sqrt{(t - t_0)}} \tag{3.b}$$

For these experiments, [36] found that on a mass-basis C_{KOSI} had a value of 2.3×10^{-5} at an input flux of 1300 Wm^{-2} and 0.5×10^{-5} at 320 Wm^{-2} where the particle flux, J_{KOSI}, is given in units of 10^{-4} g cm^{-2} s. In terms of molecules and mks units, these constants are 7.7×10^{18} molecules m kg^{-1} $s^{-0.5}$ and 1.7×10^{18} molecules m kg^{-1} $s^{-0.5}$. Most of the values obtained by curve fitting fall into this range with values of C_{KOSI} ranging from 1.2 to 13×10^{18} molecules m kg^{-1} $s^{-0.5}$. The results of these fits, along with the goodness of fit R^2 parameter (Coefficient of Determination) are documented in Table 4. Additionally, using the derived KOSI constant and equations (1.a), (2.c) and (3.a) an equation for the diffusivity of the dust mantle may be derived:

$$D_{eff} = m_{H2O} TR \frac{B\rho^2 C_{KOSI}^2}{2p_{sat}} \quad (4)$$

The values for the diffusivity of the dust lag derived in this way are also documented in Table 4 and range from $9 \times 10^{-9} m^2 s^{-1}$ to $3 \times 10^{-7} m^2 s^{-1}$ and average $1.2 \times 10^{-7} m^2 s^{-1}$. These values are too small to represent molecular diffusion through the chamber, which is of order $10^{-3} m^2 s^{-1}$ at these temperatures and pressures [37].

These diffusivities can be used to determine the average spacing of the particles by employing calculations for Knudsen diffusion through cylindrical pores between particles in the dust mantle using the formulation of [38]. These calculations give a characteristic pore size of less than an angstrom, smaller than a water molecule. However, since the particles which make up the dust lag are in actuality only a few microns in size, it was expected that pore sizes would be of similar size. Performing the Knudsen diffusion calculations for micron-sized pores gives values that are similar to the values for molecular diffusivity, namely $10^{-3} m^2 s^{-1}$. While significant tortuosity could reduce this figure, it is doubtful that sufficient tortuosity exists within a dust mantle only tens of particles thick to reduce the observed diffusivity by four orders of magnitude.

Thus, it seems unlikely that dust mantling alone is responsible for the reduction in pressure that is observed within the sample chamber. Another possibility for this trend is given by adsorption which has previously been seen to produce abnormally low effective diffusivities under certain conditions [39-41]. More evidence for this possibility comes from a consideration of the large fractionations observed. Therefore adsorption will be considered in greater detail in the Section "Dust mantle adsorption".

Heavy fractionation during sublimation

Discussion of cold trapping

Why is it that the D/H ratio of the sublimate gas decreases with time? This effect is not seen in solid samples. Depending on the rate of solid state diffusion within the sample and the rate of removal of material from the head space, solid samples may sublimate un-fractionated, i.e. at the bulk ratio of the solid as monolayer after monolayer are stripped away. Or, instead, even solid samples may exhibit a Rayleigh-like fractionation in which the head space gas becomes more isotopically heavy with time e.g. [19] if diffusion allows molecules to travel away from the actively sublimating surface faster than the sublimation front proceeds.

However, solid samples do not have direct pathways down to a cold trap which can have a temperature as much as 150 K less than the actively sublimating surface. Thus, cold trapping of HDO is an attractive possibility for producing an overabundance of the light isotope in the headspace gas. In light of the large temperature gradients that exist in the samples under consideration and the corresponding high fractionating factors predicted by the kinetic isotope effect, this mechanism for enriching the headspace gas in the light isotope must be examined.

Some insight can be gained by considering the results of the KOSI experiments along with simulations performed by [42]. In both cases, it was observed that condensable material evaporated from the surface would penetrate into the subsurface. However, due to the decrease in temperature this material recondensed quickly before travelling deeply into the sample. As such, a short distance below the surface, a peak was seen in

the diffusing material, followed by a drop-off to normal conditions in the deeper interior. This suggests that volatile transport will be localized to a layer near the surface, and that the concentration of the more refractory component, HDO, will increase at the surface due to preferential transport of the lighter, more volatile H_2O. This is exactly what has been observed in the KOSI experiments where the D/H ratio in the near surface was seen to be slightly enriched in deuterium by 47.7‰ at the end of the 34-hour KOSI-7 run [29] while the rest of the sample was unaffected.

A simple numerical simulation shows that the samples considered in this paper are no different. By altering Eq. (1.a) such that the temperature is allowed to vary and applying it to the sample interior instead of the dust mantle, the rate of diffusion and flux of H_2O and HDO through the sample can be calculated based on some simple assumptions about the geometry and kinetics. For the samples considered in this paper, a pore radius of at most 0.5 mm, corresponding to the typical size of the crushed ice-dust grains, and a temperature gradient of 30 K cm^{-1} are reasonable, which implies utilizing the Knudsen diffusion equation as the pore radius is smaller than the mean free path at these temperatures. The results are shown in Figure 6. As can be seen, the rate of transfer becomes relatively small below one centimeter from the surface. This perhaps explains why the D/H ratio appears to have been reset in the dusty runs where the top 1 cm was removed between runs (Table 2 runs 8A and 8B).

The most significant argument against implicating pathways in the fractionation process is that a trend in dustiness would not be expected for this phenomenon. There are runs when the pathways to the cold finger are present with very little dust or in the absence of dust entirely. The top panel in Figure 4 is a good example. In none of these cases was a significant fractionation observed.

Dust mantle adsorption

As such, the dust must be the source of the fractionation observed. This is supported by the observation that fractionation proceeds more rapidly when more dust is entrained in the sample. The major way in which this dust can interact with the gas and ice in the chamber is through adsorption. Previous work [39-41,43,44] on the palagonites used to simulate martian surface materials, such as JSC MARS-1 indicate that palagonites should readily interact with water vapor at low temperatures. This would explain the very low effective diffusivities observed in the Section "Pressure decline" without having to resort to high tortuosities or extremely tiny pore radii.

This behavior has been previously noted in ice sublimating through regolith [39,40] and can result in an observed effective diffusivity that is much lower than would be predicted by either molecular or Knudsen diffusion alone. The situation discussed in [40] is not dissimilar from a sublimating dusty ice which is forming a dust mantle, as is occurring in the experiments detailed in this paper. Thus, it is useful to consider the analysis from [40]. From Chevrier's equation (15) the reduction in the diffusivity can be expressed as:

$$D_{eff} = \frac{D_0}{1 + \psi \frac{\partial \theta}{\partial p}} \tag{5}$$

Where D_{eff} is the effective or observed diffusivity of the dust or regolith layer, D_0 is the diffusivity controlling the movement of vapor between dust particles, i.e. the lesser

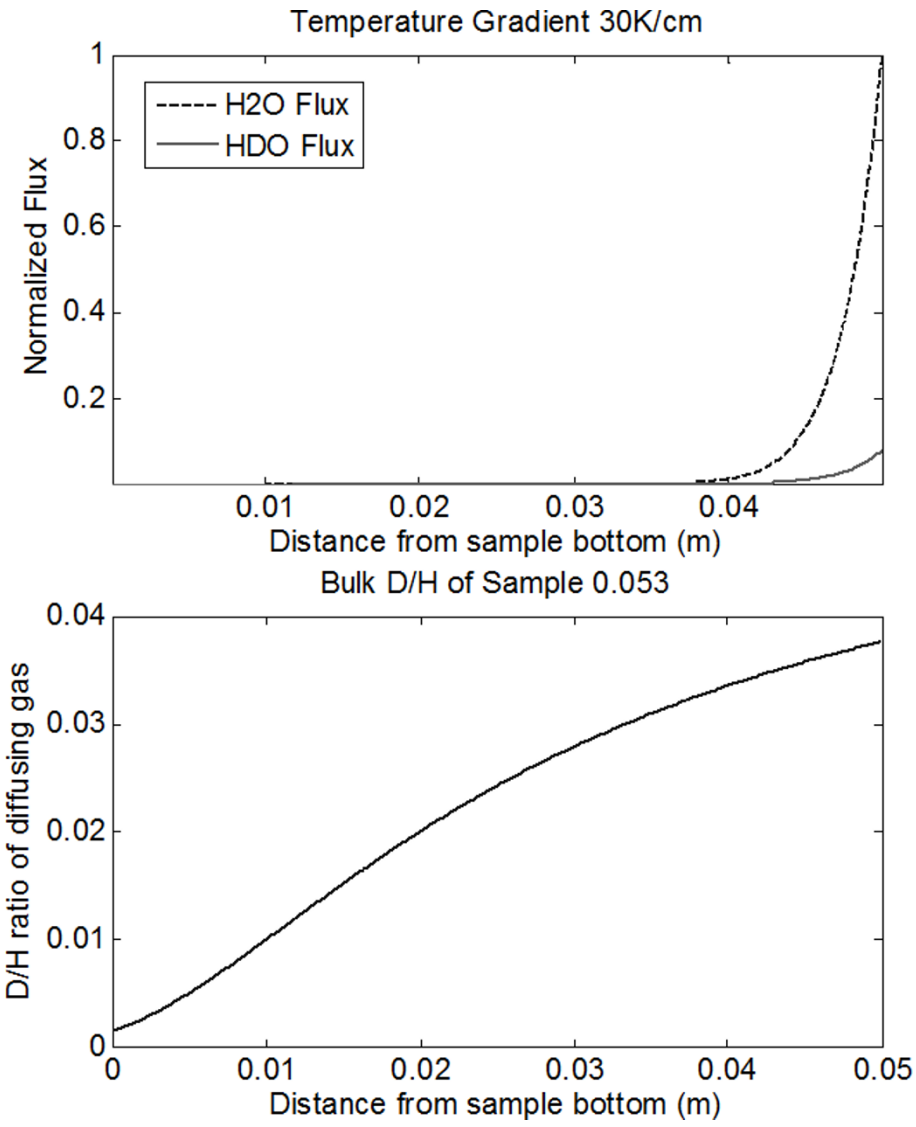

Figure 6 Numerical model results showing the normalized rate of gas diffusion at different levels and the D to H ratio of the diffusing gas in the sample at the beginning of a run with a surface temperature of 210 K and a thermal gradient of 30 K/cm. Total depth is 5 cm (0.05 m). Below 1 cm from the surface, the fluxes become very low, restricting the flow of material. As such, (1) large amounts of gas will condense out before reaching the highly fractionating bottom layers. Also, (2) since condensation greatly exceeds sublimation at depth, the inward-travelling gas is isotopically light, composed principally of H_2O.

of molecular and Knudsen diffusivities for the given situation. Ψ is a thermodynamic constant defined by [40] as equation (22) repeated below:

$$\psi = \frac{R_u T \rho_{H2O} \rho_{reg} A_S l}{M_{H2O}} \tag{6}$$

Where R_u is the universal gas constant, T is again the surface temperature of the subliming ice, M_{H2O} is the molar mass of water, 0.01802 kg mol^{-1}, l is the thickness of an adsorbed monolayer, 2.75 × 10^{-10} m, ρ_{H2O} and ρ_{reg} are the densities of the adsorbed

water layer and the regolith, respectively, 1000 kg m^{-3} and 800 kg m^{-3} and A_S is the specific surface area in m^2kg^{-1}. For the situation described in this paper, $\Psi \sim 1.4 \times 10^7$ J m^{-3}.

The last element from equation (5) is the slope of the θ-p relationship where θ is the surface coverage and p is the pressure of water vapor in contact with the regolith. The formulation of this term is slightly different from [40] equation (23) in that here particles are exhumed from solid ice by sublimation instead of starting out as dry overburden. They can therefore be considered to start out with completely filled monolayers of adsorbate under a Langmuir scheme, i.e $\theta(t = 0) = 1$. This implies (see [40] for a description of the derivation):

$$\frac{\partial\theta}{\partial p} = \frac{\alpha}{(1+\alpha p)^2}\left[1 - (k_D t(1+\alpha p) + 1)e^{-k_D(1+\alpha p)}\right] \tag{7.a}$$

Where k_D is the desorption rate constant and α is the adsorption coefficient. This equation contains the time-varying terms which have an effect on the diffusivity when the state of adsorption in the dust mantle is changing. These are particularly important for the case of dry overburden where the Langmuir isotherm is steep and the slope of the θ-p relationship is large and rapidly evolving as more and more water vapor becomes adsorbed on the surface. However, for the case in which material begins fully saturated, large reductions in the surface coverage, θ, can be achieved without changing the slope of the θ-p curve significantly. Additionally, since the limiting behavior of the system is of greatest interest, it is useful to consider the system at $t >> t_0$. Both of these criteria suggest using the following simplified form for the adsorption slope in which equation (7.a) reduces to:

$$\left.\frac{\partial\theta}{\partial p}\right|_{t>>0} = \frac{\alpha}{(1+\alpha p)^2} \tag{7.b}$$

This formulation is nearly entirely time-independent, having only a dependence on pressure. Since the effective diffusivities average close to 10^{-7} m^2 s^{-1}, and the molecular and Knudsen diffusivities for particles of this size are of order 10^{-3} m^2 s^{-1}, the value of the denominator in equation (5) is of order 10^4. This implies values for the slope of order 10^{-3} m^3 J^{-1} and values of α of either $> 10^3$ or $< 10^{-3}$ for the pressures encountered in the experimental apparatus, and the value of Ψ.

Only the larger set of these values is physical. To explain this assertion, consider that the adsorption coefficient may be expressed as the ratio of adsorptive and desorptive rate constants. At low temperatures, adsorption should be more effective and desorption should be less effective. Thus, it is expected that values for α will be several orders of magnitude greater than at higher temperatures, such as at 270 K where $\alpha \sim 0.01$-0.1 is a more common range [40] or at 243 K where $\alpha \sim 0.81$ [41]. Since α cannot be less than 0.81 at 200 K, the higher values are more appropriate.

Adsorptive Fractionation

When HDO is introduced, the situation becomes more complicated. In addition to the adsorption and desorption processes for each species, it may be necessary to consider the interactions between the two species [39] considered the effect of a two-component system on the adsorption and desorption process in their section 4.5 and show the results expected for a system with an isotopic composition of 1 HDO: 1000 H_2O

in their figure nine. They observe that significant increases in the relative surface coverage of HDO are possible whenever α_{HDO} is greater than α_{H2O}.

How will this increase in the amount of HDO adsorbed on the dust mantle affect the composition of the sublimating gas? To determine what an idealized system with an adsorptive dust lag would look like, a numerical model was created using equations (1.a) through (1.c) to simultaneously solve for the pressure of HDO and H_2O in the headspace as the dust lag thickens. These dust lag differential equations were linked to adsorption through the effective diffusivity by making use of equation (5) modified for the two component system as:

$$\boldsymbol{D}_{eff} = \boldsymbol{D}_0 \frac{1}{1 + \psi \left(\frac{\partial \boldsymbol{\theta}}{\partial p_{H2O}} + \frac{\partial \boldsymbol{\theta}}{\partial p_{HDO}} \right)} \tag{8}$$

This equation, in turn, requires information on the adsorption state, θ, of the dust lag. If it is assumed that for each thickness of the dust lag a quasi-steady (i.e., time independent adsorption at each time step) state exists in terms of the adsorption state of the dust lag, then, for the 2-component system described here, the adsorptive state at each level within the dust may be described (after [39]) by:

$$\boldsymbol{\theta} = -\boldsymbol{G}^{-1}\boldsymbol{k} \tag{9}$$

Where:

$$\boldsymbol{G} = \begin{bmatrix} -k_{H2O}^{ads} - k_{H2O}^{des} - k_{HDO}^{X} & k_{H2O}^{X} - k_{H2O}^{ads} \\ k_{HDO}^{X} - k_{HDO}^{ads} & -k_{HDO}^{ads} - k_{HDO}^{des} - k_{H2O}^{X} \end{bmatrix}, \boldsymbol{k} = \begin{bmatrix} k_{H2O}^{ads} \\ k_{HDO}^{ads} \end{bmatrix} \tag{10}$$

Note that the adsorption and desorption rate constants, k, are subscripted with the species in question and superscripted as to whether they represent rates for adsorption of a molecule on an empty site (ads), desorption of a molecule to leave an empty site (des) or the displacement of a molecule of one species by that of another (X).

If it is assumed that the temperature of the sublimating ice surface and the entire dust lag remains constant, then the desorption rate constants, k^{des}, for each component should themselves be constant. However, the adsorption coefficient will vary with pressure throughout the lag [after [40], equation (18)] according to:

$$k_{HXO}^{ads} = k_{HXO}^{des} \alpha_{HXO} p_{HXO} \tag{11}$$

Where the subscript *HXO* denotes either of H_2O or HDO. Here the desorption coefficients, k^{des}, are assumed to be equal for both species and the values used are those from [43] of approximately 1×10^{-4} s^{-1}. Next, α_{H2O} is known from equation (7.b) and α_{HDO} can be calculated from the relationship derived by [39] of $\alpha_{HDO} = \alpha_{H2O}/0.6$. Finally, for simplicity, all the substitution adsorption coefficients, k^X, are set to zero. The information from (9), (10) and (11) can be substituted back into equation (8) in order to determine the slope of the adsorption isotherm (slope of the θ-p curve).

Using this information, a fourth order Runge-Kutta (RK4) scheme was implemented to solve for the pressure of HDO and H_2O within the dust lag as a function of time. The pressure at the ice surface was assumed to be saturated at all times for both H_2O and HDO and the value of all kinetic constants were as described above. Runs were completed at several different dust concentrations ranging from 1 wt% up to 25 wt%.

A value of 7000 for α_{H2O} was selected as the time required for fractionation in the simulations using this value matched reasonably well with what was observed in Figure 5 and it satisfies the requirements of equation (7.b).

The result of this calculation, up to an elapsed time of 10 days is shown in Figure 7. The curves in Figure 7 replicate many of the features of the simulations described in the Section "Results". All show a decrease in the D/H ratio of the sublimating gas with time. Also, the higher the initial dust content, the more rapid is the rate of decrease. However, no matter the starting concentration, the end fractionation is the same, with the system asymptotically approaching a D/H value of:

$$\lim_{t\to\infty}\frac{D}{H} = \left.\frac{D}{H}\right|_{t=t_0}\frac{\alpha_{H2O}}{\alpha_{HDO}} \tag{12}$$

What does it mean for α_{HDO} to be greater than α_{H2O}? This suggests that at the same temperature, the affinity of the dust for HDO is higher than for H_2O. Since H and D have been observed in other experiments to fractionate heavily on surfaces [45,46] at low temperature, it is reasonable that HDO could be adsorptively sticky, compared to H_2O. In the case of H_2 and HD this assumption is a common one i.e. [47] and is often a starting point in considering exchange on the surfaces of dust grains that further sequester the deuterated species.

As far as fractionation is concerned, a larger α_{HDO} implies a smaller $D_{HDO}{}^{eff}$. This means that as gas passes through the dust, HDO is impeded more than is H_2O. As a result of this adsorptive separation, a stable fractionation can be obtained between the two gasses, as described by Eq. (12). Adsorption provides an effective mechanism for achieving this fractionation due to the gradient that will exist within the dust lag layer. Newly exhumed particles emerge with all adsorption sites filled, but over time this

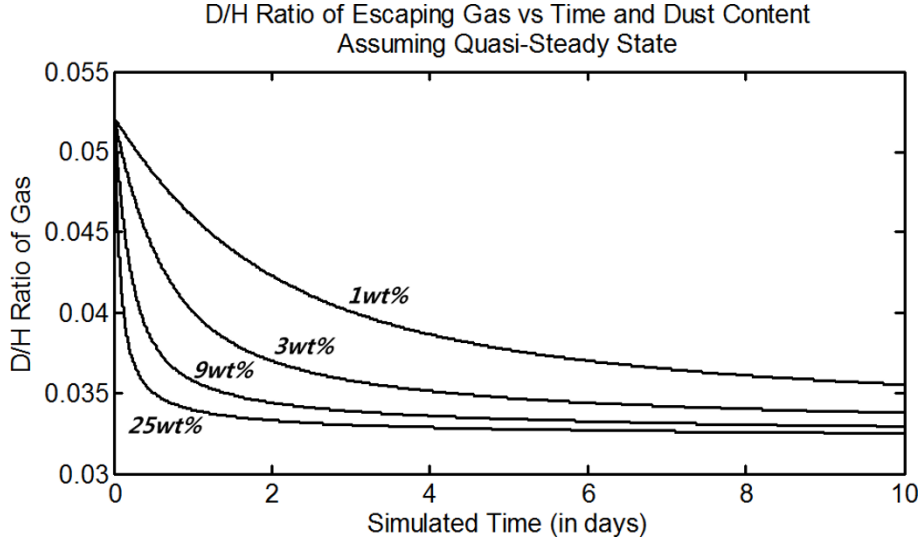

Figure 7 Numerical Model runs describing the D/H ratio of the sublimating gas as a function of time and dustiness for the H_2O-HDO system and starting concentrations relevant to the experiments documented in Figure 5. Substitution is assumed negligible. The value of α_{HDO} is set at α_{H2O} /0.6. The dustier the original starting material the faster each curve approaches the limiting value of D/H = α_{H2O} /α_{HDO} = 0.6 $(D/H)_0$. Different values for α_{H2O} will produce different timescales for reaching the asymptotic D/H ratio. A reasonable value, 7000, is shown here.

material is lost. Since the lag particles remain at the same temperature, this cold dust readily adsorbs molecules attempting to transit the layer. Later on these molecules are released through desorption in a mechanism similar to scattering. This adsorption-desorption process increases the transit time of molecules through the layer, giving rise to the very high apparent diffusivities observed. The closer the molecules are to the surface of the lag, the fewer adsorption sites are filled and the greater is this effect. Over time, as the lag thickens, the gradient in θ increases until, ultimately, the pressure of each species in the headspace reflects the affinity of the lag for each species rather than the difference in sublimation rates at the solid ice surface.

Finally, a note of caution is required. The apparatus and experimental method employed was chosen primarily for its ability to represent a realistically sublimating dusty surface and included all the imperfections inherent in such an experiment. It was not selected for the ability to precisely examine the kinetics of adsorption and to provide specific constants at low temperature.

Using adsorption to explain a special case

The framework developed in sections "Dust mantle adsorption" and "Adsorptive fractionation" can be used to explain the major differences in behavior between the 9 wt% run depicted in Figure 5E and the 25 wt% run depicted in Figure 5F. While both tend towards similar values for the D/H ratio in the long term, Figure 5E shows a declining trend after lamp illumination whereas Figure 5F shows an increasing trend. To understand how both cases can be explained by an adsorptive framework it is necessary to consider the cold illumination-free state before the initial lamp-on state. Initially, the ice begins by sublimating near the bulk D/H ratio. However, as dust is exhumed from the ice-dust matrix, water that has been adsorbed to that dust at the bulk ratio attempts to reach a new equilibrium. HDO is preferred by the dust and therefore replaces H_2O on dust grain surfaces and which is manifested as a progressive decline in the D/H ratio of the gas as the dust lag builds and scavenges HDO from the gas phase. This trend is seen in Figure 5F and several other runs including those depicted in Figures 5B, D and 5E prior to lamp illumination. In those three last runs, the process is short circuited at this point by the illumination of the lamp.

But for the run shown in Figure 5F, so much dust lag is exhumed prior to lamp illumination that the adsorption state of the dust evolves further. Eventually, the dust lag grows thick enough that it is does not only provide surfaces for adsorption, but is able to control the flow of gas from the subsurface. At this time a local equilibrium state is achieved at each level within the dust lag. As the gas in the headspace is HDO-poor compared to the ice surface, more and more HDO must be adsorbed on dust the lower that dust is within the lag, i.e. the closer that dust is to the ice. This acts to sequester HDO close to the ice layer.

However, this situation cannot persist. As the concentration of HDO increases at the base of the lag layer, the equilibrium at each level shifts towards greater and greater concentrations of HDO in the gas phase until, ultimately, the emitted gas from the top level has the same concentration as the gas supplied to the bottom of the dust lag. Thus, in the absence of illumination eventually a steady state is achieved with sublimation occurring at the bulk ratio. This typical transitory behavior of adsorptive systems is described well by [40] and was also seen in [39] and occurs when a stable dust lag or regolith evolves to a steady adsorption state throughout.

What happens when the lamp is illuminated? Immediately, the volume of gas sublimating from the ice surface increases by over an order of magnitude due to the sudden increase in temperature. But since the lag layer is already fully developed, of order 100 μm in thickness, the backpressure causes this ice to sublimate at the equilibrium ratio given by the Kinetic Isotope Effect (α ~1.3 at these temperatures [15]). After passing through the lag layer, the gas is further fractionated by adsorption (α = 1.7 at these temperatures [39]) which results in the first emitted gas having a D/H ratio of ~0.025.

It is the lamp that keeps the top of the lag layer in a low-θ state that allows it to continue to fractionate gas. Over time, the D/H ratio of the gas emitted from the top of the dust lag will increase until only the fractionation from the dust is present. The advancing sublimation front within the solid ice provides new material to the system at the bulk ratio. Thus the maximum fractionation is the dust lag fractionation multiplied by the bulk ratio. Interestingly, this implies that the D/H ratio at the dust lag/ice interface is larger than the bulk ratio by the amount specified by the kinetic isotope effect (i.e. 0.069 at the top of the solid ice layer).

The D/H ratio of the sublimation cascades suggests that this layer of enriched ice is thin compared to the thickness of ice that is consumed by a cascade. This can be shown by assuming that a significant amount of material is rapidly vaporized. If the enriched layer is small, on the average, this material will have close to a bulk composition. But since it is trapped underneath the dust lag by significant backpressure, HDO will recondense until the gas plug D/H ratio is equal to the value given by KIE. This gas then makes its way through the dust lag and is fractionated further, emerging with a D/H value close to 0.025 which is close to the peak values of D/H observed for these cascades.

Implications for sublimating water ice on icy bodies

General implications

For bodies containing significant amounts of dust, preferential adsorption of HDO means that the solid is able to hold onto more deuterium than is predicted by the Kinetic Isotope Effect [48]. As a result, more fractionation can take place between the ice reservoir and the sublimate gas. Therefore the observed concentration of HDO in the sublimate gas will be lower than expected, or the source material will be richer in HDO than expected, depending on which planetary reservoir is being observed. In either case, the key to determining the significance of this experimental result on our understanding of the history of water in the solar system hinges on our knowledge of the plausible cycling between different reservoirs in a planetary setting and the pressure and temperature conditions under which the cycling occurs.

There are a great number of icy bodies in the solar system, but of these, this effect is likely to be significant mainly for two examples: Comets and the Martian polar caps. While the icy moons certainly contain large amounts of water ice, the vapor pressures involved are too small to mobilize this material, even over the timescale of the solar system, and their surfaces do not suggest large amounts of contaminating dust. Comets outgas heavily as they pass through the inner solar system and are known, from spectroscopy and space missions e.g. [49-51], to contain a great deal of dusty material. The polar caps of Mars are also known to be rich in dust [52] with up to 6% by weight on

the surface, as determined by the OMEGA instrument on Mars Express [53] and potentially more at depth.

Comets

In some ways, the experiments discussed in this paper are a good analogue of a comet. Porosity estimates of the water ice grains produced in our experiments were, typically, near 40% or higher which is consistent with the data on cometary nuclei [54]. As well, the temperatures simulated in the lab were analogous to surface temperatures seen on comets, with back-pressures of about a Pa or less. The major differences between the experiment and reality are twofold. First the typical temperature gradient of 30 K cm^{-1} is likely far higher than what can be expected on comets. This means that, in contrast to our results, it is possible that there could be significant cold trapping if vapor is able to penetrate to depth within the comet. As well, comets likely have a layer of dry overburden much thicker than the fraction of a millimeter present by the end of the experimental runs described herein.

Comets are thought to represent early solar system materials, perhaps being made up of ice originally condensed from the solar nebula which has not since been processed or transported to another reservoir. As such, the isotopic composition of comets should be indicative of material present in the early solar system. It is in light of this information that the high value of the D/H ratio for most cometary coma, twice VSMOW [8-10,55], is puzzling. This value is enriched significantly compared to most other solar system reservoirs and represents an enrichment of almost 15 times compared to inferred protosolar values. Much of the work to date has, understandably, focused on attempting to explain how the observed enriched values of D/H in the coma could imply a much lower HDO concentration in the nucleus i.e. [56]. One of the main questions driving this debate is the source of water on the terrestrial planets. If comets are enriched in HDO compared to the earth, it becomes very difficult to form a set of circumstances under which a significant fraction of the Earth's water can be delivered by comets [1]. Recent observations by [55] of a D/H value near 1.0 times VSMOW in comet 103P/Hartley 2 has drawn this debate into sharper focus.

The results obtained from our sublimation experiments in the laboratory offer a potential solution. Since it seems likely that the heavier isotope is being concentrated on the dust, different values for the D/H ratio will be obtained depending on the provenance of the water vapor used for analysis. If that water vapor has been desorbed from dust grains, it is likely to have a higher D/H ratio than solid buried cometary ice. This will be especially true near the start of any degassing cycle before the comet has reached perihelion. Thus the D/H values obtained for comets in flybys of comae may not be at all representative of the reservoirs from which those comets formed depending on the stage of outgassing at which those comets are observed.

In order to better constrain the fractionation processes occurring on and near comets both spacecraft and ground-based observations are necessary [19] showed that the D/H ratio in sublimated gas can vary with distance from the cometary nucleus, increasing with distance. One possible reason for this trend might be that high-D/H material adsorbed on dust grains is evaporating as the grains are progressively dehydrated in their passage away from the comet. In order to understand this process, a spacecraft capable of measuring D/H would ideally provide measurements along a profile from the outer coma all the way to the surface of the nucleus.

Ground-based spectroscopy would also be helpful. To date, seven comets have been observed and their D/H values measured [55] but each was observed for only a few nights. While these measurements varied from 37 days before perihelion for comet Hyakutake [9] to 27 days past perihelion for comet 2002 T7 (LINEAR) [57] no comet has yet been observed over a long period which might show an evolution in the D/H ratio of the water vapor contained within the coma. D/H ratios within those comets vary significantly with six clustered near 1.9 times VSMOW and one near 1.0 times VSMOW [55]. This variation is comparable to the variation that can be imposed by adsorption on dust as discussed in the current paper. Therefore, long-term measurements of the evolution of the water in the coma could help to determine whether these snapshots of D/H are representative of the water in the nucleus.

Mars

Unlike a comet, the history of Mars contains numerous transfers between different reservoirs. As such, there is an extensive literature studying the D/H history of the planet in terms of plausible volatile cycling histories [58]. All routes from these ancient sources of water lead to the present-day polar caps where most of the modern surface ice currently resides [52]. Even here, the cap is marked by numerous layers and unconformities recording many advances, retreats, and additions to the ice cap which may be linked to past climate cycles [59]. These ice caps are themselves highly enriched in dust [52]. This dust is most likely similar in character to the atmospheric particles which cover the planet. These particles average 1.6 microns in radius as determined from the Imager for Mars Pathfinder [32] and Mars Exploration Rover missions [31] and are similar in spectra and composition to JSC Mars-1 analog, the dust simulant used in our experiments.

An additional advantage when considering Mars is the availability of fossil D/H ratios from martian meteorites. The oldest of these, the nahklites, chassigny and ALH 84001, all show relatively low D/H ratios of between 1 and 2 times VSMOW [60]. Since these meteorites are basaltic, it is presumed that the trapped water represents the primordial water of the Martian mantle which is likely representative of the initial D/H ratio of Martian water in general. Furthermore, the overall composition of the trapped water in QUE94201, a more recently formed shergotite, can be decomposed into a mixture of two sources, the first with a ratio of 1.9 times VSMOW assumed to be representative of the interior, and the second with a ratio of 5.2 times VSMOW, thought to be representative of the atmosphere [61].

A potential compounding factor is Carbon Dioxide. This will reduce the number of available sites for adsorption as all three gasses compete for a fixed amount of surface area. However, it has been found experimentally that water vapor is able to displace adsorbed CO_2 [62] and so this is expected to have little effect. The presence of CO_2 will also restrict the flow of molecules, however, it should be noted that the values of the diffusivity listed here are already much smaller than typical martian regolith diffusivities measured in the lab e.g. [40].

It is common practice that in the Knudsen regime, the molecular diffusivity of any additional interstitial gas can be ignored e.g., [38] since collisions occur much more frequently with the walls. This situation will change drastically once molecules have escaped the surface of the material, as molecular diffusion will dominate. Here advection of water vapor from the surface becomes important, as any back pressure will

tend to restrict the diffusion rate by changing the pressure drop across the regolith. However, models have suggested that advection of the lighter H_2O and HDO in the heavier CO_2 on Mars may be more effective than sublimation into an atmosphere of pure water vapor [63] based on [64]. In fact, considering the model of [65], the typical advected flux at 203 K (H_2O pressure of ~0.5 Pa) is approximately 1.1×10^{16} molecules s^{-1} m^{-2}. This is comparable to the range of escape rates seen in the apparatus at this temperature of 1×10^{16} to 4×10^{18} molecules s^{-1} m^{-2}. As such, the results should be applicable to the Martian situation.

In the literature, present-day sublimation on Mars has only rarely been concerned with isotopic differences. Here, there are two schools of thought. The first of these is to consider ice on Mars as a continuously well mixed reservoir as one might consider the Earth's ocean [17] took this approach when they calculated total fractionation effects from surface to space [18] took a different approach, considering the opposite case in which no net fractionation occurred. Both of these models were attempts to use the enriched D/H ratio of Mars today to determine the size of the exchangeable water reservoir and both papers made important contributions [17] do an excellent job of characterizing the fractionation of the atmosphere to space, which is significant and has since been further refined e.g. [66-70] while [18] does an excellent job of quantifying the overall infalling water fluxes. However, neither model examined surface fractionation upon sublimation in detail. As such, our results provide the missing piece in the analysis.

Sublimation can itself bring about fractionation in surface reservoirs, as our results show, and much of the highly enriched material will remain close to the surface, likely adsorbed onto dust. As water moves on Mars mainly by vapor phase mechanisms, the enriched dust will gradually increase the amount of HDO present in the surface reservoir. Thus it is possible to imagine plausible scenarios in which Mars could appear to have a high-Deuterium surface and atmosphere without having lost as much water as would be required without the action of adsorbing dust. As such, direct sampling of the surface and subsurface water reservoirs is required to determine the bulk ratio, with coring of the polar cap being even more attractive as a means to deconvolve the isotopic effects of repeated volatile cycling over geologic time.

Conclusions

Sublimation experiments have been carried out to determine the effect of mixing dust with porous ice on the isotopic composition of the sublimate gas. Disaggregated samples, in particular, were produced with high porosities by flash freezing in liquid nitrogen and crushing to sand (mm) sized particles. When dust was incorporated in the mixture to be flash frozen, the D/H ratio of the sublimate gas was seen to decrease with time from the bulk ratio. The more dust was added to the mixture, the more pronounced was this effect.

Two possible mechanisms for producing this effect were identified, migration of material within the sample and adsorption on dust grains. Simple models for migration of HDO within the sample were prepared which included sublimation, condensation and vapor diffusion. However, these showed that it is very difficult to sequester isotopically heavy material at depth. This suggests that adsorption within a thickening dust mantle is a better mechanism for separating HDO and H_2O. This is bolstered by the

fact that identical samples without dust did not fractionate. As well, without adsorption on dust the diffusivities observed within the dust mantle are too low to be credible.

A close examination of the binary adsorptive system showed that a difference in the adsorption coefficients of H_2O and HDO reproduces many of the attributes of the fractionating system. The model simulations are able to reproduce an increasing fractionation in the D/H ratio of the system with time and with increasing dust mixing ratio. The ratio of the adsorption coefficients can be determined from the fractionation to which the system asymptotes. For JSC Mars-1 near 200 K, an adsorption coefficient of HDO larger than that of H_2O by a factor of 0.6, i.e. $\alpha_{HDO} = \alpha_{H2O}/0.6$ as seen by [39] reproduces the observed trend in dust.

These results imply that dusty porous ices are more able to retain HDO than are clean porous ices. This has significance for the major reservoirs of sublimating dusty ices in the solar system; comets and the martian polar caps. In both cases, measurements of sublimated gas alone have been made and from these measurements a bulk ratio in the solid has been inferred. This work suggests that the estimates of the bulk ratios of these bodies need to be adjusted for the action of dust and must therefore take into account the history of volatile cycling on each body. As such, the dusty surfaces of comets may contain more deuterated material than their interiors making a determination of the primordial D/H ratio of cometary water from measurements made in cometary comae difficult at best. As for Mars, given plausible histories of water cycling on the planet, scenarios in which the atmospheric D/H ratio bears little resemblance to the bulk ratio of martian water are possible. As such, Mars may possess a greater fraction of its original water than previously considered possible.

In both cases, this work highlights the need for further experiments to determine the kinetic constants of adsorption and for ground truth. In particular, experiments which seek to determine the specific adsorption kinetic constants as a function of temperature down to 150 K would be highly valuable in further numerical modeling. In terms of ground truthing, only direct sampling of Martian and Cometary water will be able to reliably determine the D/H ratios of the different reservoirs. In fact, for Mars, coring of the polar ice cap may be necessary in order to determine typical values if the deposits of water ice are isotopically stratified from repeated cycling, as seems likely. Furthermore, measurements of D/H in comets that cover as much of the cometary orbit or atmosphere as possible could be used to shed light on the nature of water adsorbed on cometary regolith.

Acknowledgements
This work was partially supported by a scholarship provided by the Natural Sciences and Engineering Research Council of Canada (NSERC).

Author details
[1]Lunar and Planetary Laboratory, Department of Planetary Sciences, University of Arizona, 1629 E University Blvd, Tucson, AZ 85721-0092, USA [2]Now at: Centre for Planetary Science and Exploration, Department of Physics and Astronomy, University of Western Ontario, 1151 Richmond Street, London, ON N6A 3 K7, Canada

Authors' contributions
JEM carried out the experiments, data reduction and theory described in this paper under the advice and council of RHB, DSL and PHS. The experimental apparatus and operating time was provided by RHB and DSL. Materials were acquired with the help of RHB, PHS and DSL. All authors read and approved the final manuscript.

Competing interests
The authors declare that they have no competing interests.

Received: 23 August 2011 Accepted: 20 April 2012 Published: 20 April 2012

References

1. Drake MJ: **Origin of Water in the Terrestrial Planets.** *Meteoritics and Planetary Science* 2005, **40**:519.
2. Hunten DM: **Atmospheric Evolution of the Terrestrial Planets.** *Science* 1993, **259**:5097, 915-920.
3. Owen T, Maillard JP, de Bergh C, Lutz BL: **Deuterium on Mars: the Abundance of HDO and the value of D/H.** *Science* 1988, **240(4860)**:1767-1770.
4. Krasnopolsky VA: **High-resolution spectroscopy of Mars at 3.7 and 8 μm: A sensitive search of H_2O_2, H_2CO, HCl, and CH_4, and detection of HDO.** *J Geophys Res* 1997, **102**:6525-6534.
5. Hunten DM, Pepin RO, Walker JCG: **Mass Fractionation in Hydrodynamic Escape.** *Icarus* 1987, **69**:532-549.
6. Geiss J, Gloeckler G: **Composition of H, He, and Ne in the protosolar cloud.** *Space Science Revs* 2003, **106**:3-18.
7. Vanysek V: **Isotopic Ratios in Comets.** In *Comets in the Post-Halley Era.* Edited by: Newburn RL, Neugerbauer M, Rahe J. Kluwer, Dordrecht, The Netherlands; 1991:299-311.
8. Eberhardt P, Reber M, Krankowsky D, Hodges RR: **The D/H and O^{18}/O^{16} ratios in water from comet P/Halley.** *Astronomy and Astrophysics* 1995, **302**:301-316.
9. Bockelee-Morvan D, Gautier D, Lis DC, Young K, Keene J, Phillips T, Owen T, Crovisier J, Goldsmith PF, Bergin EA, Despois D, Wootten A: **Deuterated water in comet C/1996 B2 (Hyakutake) and its implications for the origin of comets.** *Icarus* 1998, **133**:147-162.
10. Meier R, Owen TC: **Cometary Deuterium.** *Space Sci Rev* 1999, **90**:33-43.
11. Gat JR: **Oxygen and hydrogen isotopes in the hydrological cycle *Annu.*** *Rev Earth Planet Sci* 1996, **24**:225-262.
12. Matsuo S, Knuiyoshi H, Miyake Y: **Vapor pressure of ice containing D_2O.** *Science* 1964, **145(363)**:1454-1455.
13. Merlivat L, Nief G: **Fractionnement isotopique lors des changements d'état solide-vapeur et liquide-vapeur de l'eau à des temperatures inférieures à 0°C.** *Tellus* 1969, **19**:122-127.
14. Daansgard W: **Stable isotopes in precipitation.** *Tellus* 1964, **16**:436-468.
15. Van Hook WA: **Vapor pressures of the isotopic waters and ices.** *J of Phys Chem* 1967, **72**:1234-44.
16. Van Hook WA: **Vapor pressure isotope effect in aqueous systems. III. The Vapor Pressure of HOD (-60° to 200°).** *J of Phys Chem* 1972, **76**:3040-3043.
17. Yung YL, Wen J-S, Pinto JP, Pierce KK, Allen M: **HDO in the Martian Atmosphere: Implications for the abundance of Crustal Water.** *Icarus* 1988, **76**:146-159.
18. Carr M: **D/H on Mars: Effects of Flood, Volcanism, Impacts and Polar Proceses.** *Icarus* 1990, **87**:210-227.
19. Brown RH, Lauretta DS, Schmidt B, Moores JE: **Experimental and Theoretical Simulations of Ice Sublimation with Implications for the Chemical, Isotopic and Physical Evolution of Icy Objects.** *Planetary and Space Science* 2012, **60(1)**:166-180, doi: 10.1016/j.pss.2011.07.023.
20. Sears DWG, Kochan HW, Huebner WF: **Laboratory simulation of the physical processes occurring on and near the surfaces of comet nuclei.** *Meteoritics & Planetary Science* 1999, **34(4)**:497-525.
21. Huebner WF: **The KOSI experiments.** *Geophys Res L* 1991, **18(2)**:243-244.
22. Kochan H, *et al*: **Comet simulation experiments in the DFVLR space simulators.** *Advances in Space Research* 1989, **9(3)**:113-122.
23. Gruen E, Kochan H, Seudenstickler KJ: **Laboratory Simulation: A tool for comet research.** *Geophysical Research Letters* 1991, **18**:245-248.
24. Gruen E, Benkehoff J, Heidrich R, Hesselbarth R, Kohl H, Kuhrt E: **Energy Balance of the KOSI-4 experiment.** *Geophysical Research Letters* 1991, **18**:253-256.
25. Gruen E, Bar-Nun A, Benkhoff J, Bischoff A, Dueren H, Hellmann H, Hesselbarth P, Keller HU, Klinger J: **Laboratory simulation of comet processes: Results from the first KOSI experiments.** In *In Comets in the Post-Halley Era.* Edited by: Newburn RL, Neugebauer M, Rahe J. Dordrecht, The Netherlands: Kluwer; 1991:277-297.
26. Gruen E, Benkhoff J, Gebbhard J: **Past, present and future KOSI comet simulation experiments.** *Ann Geophysicae* 1992, **10**:190-197.
27. Gruen E, Gebhard J, Bar-Nun A, Benkhoff J, Dueren H, Eich G, Hische R, Huebner WF, Keller HU, Klees G: **Development of a dust mantle on the surface of an isolated ice-dust mixture: Results from the KOSI-9 experiment.** *J Geophys Res* 1993, **98**:15,091-15,104.
28. Seidensticker KJ, Kochan H, Mohlmann D: **The DLR small simulation chamber: A tool for cometary research in the lab.** *Advances in Space Research* 1995, **15(1)**:29-34.
29. Roessler K, Eich G, Klinger E, Trimborn P: **Changes of Natural isotopic abundances in the KOSI comet simulation experiments.** *Ann Geophysicae* 1992, **10**:232-234.
30. Allen CC, Jager KM, Morris RV, Lindstrom DJ, Lindstrom MM, Lockwood JP: **JSC Mars-1: A Martian soil simulant.** *Proc Conf Amer Soc Civil Engineering* 1998, **469-476, Space 98.**
31. Lemmon MT, *et al*: **Atmospheric imaging results from the Mars Exploration Rovers: Spirit and Opportunity.** *Science* 2004, **306(5702)**:1753-1756.
32. Tomasko MG, Doose LR, Lemmon M, Smith PH, Wegryn E: **Properties of dust in the martian atmosphere from the Imager for Mars Pathfinder.** *J Geophys Res* 1999, **104(E4)**:8987-9007.
33. Pollack JB, Ockert-Bell ME, Shepard MK: **Viking Lander image analysis of Martian atmospheric dust.** *J Geophys Res* 1995, **100(E3)**:5235-5250.
34. Satoh H, Furukawa Y, Tsukamoto K: **Isotope Segregation during Ice crystallization Process.** *Nippon Kessho Seicho Gakkaishi* 2004, **31(3)**:284.
35. Lehmann M, Siegenthaler U: **Equilibrium Oxygen and Hydrogen Isotope Fractionation between Ice and water.** *Journal of Glaciology* 1991, **37(125)**:23-26.
36. Ibadinov KhI, Rahmonon AA, ASh Bjasso: **Laboratory simulation of comet structures.** In *Comets in the Post-Halley Era.* Edited by: Newburn RL, Neugerbauer M, Rahe J. Dordrecht: Kluwer; 1991:299-311.
37. Wallace D, Sagan C: **Evaporation of ice in planetary atmospheres: Ice covered rivers on Mars.** *Icarus* 1979, **39**:385-400.
38. Clifford SM, Hillel D: **The stability of ground ice in the equatorial region of Mars.** *J Geophys Res* 1983, **88**:2456-2474.

39. Moores JE, Smith PH, Boynton WV: **Adsorptive Fractionation of HDO on JSC MARS-1 during Sublimation with Implications for the Regolith of Mars.** *Icarus* 2011, **211(2)**:1129-1149, doi:Doi: 10.1016/j.icarus.2010.10.020.
40. Chevrier V, Ostrowski DR, Sears DWG: **Experimental study of the sublimation of ice through and unconsolidatyed clay layer: Implications for the stability of ice on Mars and the possible diurnal variations in atmospheric water.** *Icarus* 2008, **196**:459-476.
41. Beck P, Pommerol A, Schmidt B, Brissaud O: **Kinetics of water adsorption on minerals and the breathing of the Martian regolith.** *J Geophys Res* 2010, **115**:E10011, doi: 10.14029/2009JE003539.
42. Hesselbarth P, Kankowsky D, Lammerzahl P, Mauersberger K, Winkler A, Hsiung P, Rossler K: **Gas release from ice/dust mixtures.** *Geophys Res L* 1991, **18**:269-272.
43. Jänchen J, Morris RV, Bish DL, Janssen M, Hellwig U: **The H_2O and CO_2 adsorption properties of phyllosilicate-poor palagonitic dust and smectites under martian environmental conditions.** *Icarus* 2009, **200**:463-467, doi:10.1016/j.icarus.2008.12.006.
44. Pommerol A, Schmitt B, Beck P, Brissaud O: **Water sorption on martian regolith analogs: Thermodynamics and near-infrared reflectance spectroscopy.** *Icarus* **204(1)**:114-136, doi: 10.1016/j.icarus.2009.06.013.
45. Koehler BG, Mak CH, Arthur DA, Coon PA, George SM: **Desorption kinetics of hydrogen and deuterium from Si(111) 7 × 7 studied using laser-induced thermal desorption.** *J Chem Phys* 1988, **89**:1709, doi:10.1063/1.455117.
46. Hoogers G, Lesiak-Orowska B, King DA: **Diffusion on a stepped surface: H and D on Rh332.** *Surface Science* 1995, **327**:47, doi:10.1016/0039-6028(94)00825-6 DOI:dx.doi.org.
47. Lipshtat A, Biham O, Herbst E: **Enhanced production of HD and D_2 molecules on small dust grains in diffuse clouds.** *Monthly Notices of the Royal Astronomical Society* 2004, **348(3)**:1055-1064, doi:doi: 10.1111/j.1365-2966.2004.07437.x.
48. Criss RE: *Principle of Stable Isotope Distribution* New York, NY: Oxford University Press; 1999.
49. Brownlee D, *et al*: **Comet 81P/Wild 2 Under a Microscope.** *Science* 2006, **314(5806)**:1711-1716, doi:DOI: 10.1126/science.1135840.
50. Burnett DS: **NASA Returns rocks from a comet.** *Science* 2006, **314(5806)**:1709-1710, doi:DOI: 10.1126/science.1137084.
51. Jorda L, Lamy P, Faury G, Keller HU, Hviid S, Kuppers MM, Koschny D, Lecacheux J, Gutierrez P, Lara LM: **Properties of the dust cloud caused by the Deep Impact experiment.** *Icarus* 2006, **187**:208-219.
52. Clifford SM, *et al*: **The State and Future of Mars Polar Science and Exploration.** *Icarus* 2000, **144**:210-242.
53. Langevin Y, Poulet F, Bibring J-P, Schmitt B, Douté S, Gondet B: **Summer Evolution of the North Polar Cap of Mars as Observed by OMEGA/Mars Express.** *Science* 2006, **307(5715)**:1581-1584.
54. Rickman H: **The nucleus of comet Halley: Surface structure, mean density, gas and dust production.** *Advances in Space Research* 1989, **9(3)**:59-71.
55. Hartogh P, Lis DC, Brokelée-Morvan D, de Val-Borro M, Biver N, Kuppers M, Emprechtinger M, Bergin EA, Crovisier J, Rengel M, Moreno R, Szutowicz S, Blake GA: **Ocean-like water in the Jupiter-family comet 103P/Hartley 2.** *Nature* 2011, **478(7368)**:218-220, doi:10.1038/nature10519.
56. Podolak M, Mekler Y, Prialnik D: **Is the D/H ratio of the Comet Coma equal to the D/H ratio in the Comet Nucleus?** *Icarus* 2002, **160**:208-211.
57. Hutsemekers D, Manfroid J, Zucconi JM, Arpigny C: **The (OH)-O-16/(OH)-O-18 and OD/OH isotope ratios in comet C/2002 T7 (LINEAR).** *Astronomy and Astrophysics* 2008, **490**:L31-L34.
58. Yung YL, Kass DM: **Deuteronomy?: A Puzzle of Deuterium and Oxygen on Mars.** *Science* 1998, **280(5369)**:1545-1546.
59. Laskar J, Levrard B, Mustard JF: **Orbital forcing of the martian polar layered deposits.** *Nature* 2002, **419**:375-377.
60. Leshin LA, Hutcheon ID, Epstein S, Stolper EM: **Water on Mars: Clues from Deuterium/Hydrogen and Water Contents of Hydrous Phases in SNC Meteorites.** *Science* 1994, 265 n°5168 86-90.
61. Leshin LA: **Insights into martian water reservoirs from analyses of martian meteorite QUE94201.** *Geophys Res L* 2000, **27**:14, 2017-2020.
62. Zent AP, Quinn RC: **Simultaneous adsorption of CO2 and H2O under Mars-like conditions and application to the evolution of the Martian climate.** *J Geophys Res* 1995, **100(E3)**:5341-5349.
63. MacClune KL, Fountain AG, Kargel JS, MacAyeal DR: **Glaciers of the McMurdo dry valleys: Terrestrial analog for Martian polar sublimation.** *J Geophys Res* 2003, **108(E4)**:5031, doi:doi: 10.1029/2002JE001878.
64. Ingersol AP: **Mars: occurrence of liquid water.** In *Planetary Atmospheres.* Edited by: Sagan et. Al. Springer Verlag New York; 1971:247-250.
65. Toon OB, Pollack JB, Ward W, Burns JA, Bilski K: **The astronomical theory of climactic change on Mars.** *Icarus* 1980, **44**:552-607.
66. Fouchet T, Lellouch E: **Vapor Pressure Isotope Fractionation Effects in Planetary Atmospheres: Applications to Deuterium.** *Icarus* 2000, **144**:114-123.
67. Bertaux JL, Montmessin F: **Isotopic fractionation through water vapor condensation: The Deuteropause, a cold trap for deuterium in the atmosphere of Mars.** *J Geophys Res* 2001, **106(E12)**:32,879-32,884.
68. Krasnopolsky VA: **Mars' upper atmosphere and ionosphere at low, medium and high solar activities: Implications for evolution of water.** *J Geophys Res* 2002, **107(5128)**:E12, doi:doi: 10.1029/2001JE001809.
69. Cheng B-M, Chew EP, Liu C-P, Bahou M, Lee YP, Yung YL, Gerstell MF: **Photo-induced fractionation of water isotopomers in the martian atmosphere.** *Geophys Res L* 1999, **26(24)**:3657-3660.
70. Miller CE, Yung YL: **Photo-induced isotopic fractionation.** *J Geophys Res* 2000, **105(D23)**:29,039-29,051.

doi:10.1186/2191-2521-1-2
Cite this article as: Moores *et al.*: Experimental and theoretical simulation of sublimating dusty water ice with implications for D/H ratios of water ice on Comets and Mars. *Planetary Science* 2012 **1**:2.